Physics – Uspekhi **45** (7) 719 – 752 (2002)

REVIEWS OF TOPICAL PROBLEMS PACS numbers: 92.10.Hm, 92.60.We, 92.70.Gt

Periodic weather and climate variations

V V Ivanov

DOI: 10.1070/PU2002v045n07ABEH000948

Contents

Abstract. Variations in meteorological parameters are largely due to periodic processes and can be forecast for several years. Many such processes are related to astronomical factors such as the gravitational influences of the Moon and the Sun, and the modulation of solar irradiance by lunar and planetary motion. The Moon, Jupiter, and Venus have the strongest effect. These influences produce lines in the spectra of meteorological variations, which are combinations of the harmonics of the frequencies of revolution of the planets, the Earth, and the Moon around the Sun with the harmonics of the lunar revolution around the Earth. Due to frequency differences between the orbital and radial motions, fine spectral features of three types appear: line splitting, line-profile complications due to radial oscillations, and additional lines due to the combination of radial-oscillation frequencies with perturbation harmonics.

V V Ivanov Institute of Marine Geology & Geophysics, Far-Eastern Branch of the Russian Academy of Science
ul. Nauki 5, 693002 Yuzhno-Sakhalinsk, Russian Federation
Tel. (7-4242) 79 61 54
E-mail: VL_Ivanov@mail.ru

Received 29 January 2001, revised 20 October 2001
Uspekhi Fizicheskikh Nauk **172** (7) 777 – 811 (2002)
Translated by Yu V Morozov; edited by A V Getling

1. Introduction

Studies of empirical spectra by computation of periodograms from long-term series of the atmospheric temperature and pressure reveal highly indented curves. The peaks of such curves are commonly regarded as spurious, arising from the specific properties of the spectra. Sea-level fluctuations are an exception, many of their elements being described as an oscillatory process [1]. Such an approach restricts the use of observations and underlies the known prejudice that the observed variations are random, being a manifestation of a natural law rather than a matter-of-course consequence of our inability to understand complicated phenomena [2]. This prejudice gives reason for the representation of the results of spectral computation strongly smoothed and with the confidence interval estimated [3]. However, a representation based on a random-process model is of little informational value. In physical measurements, the overwhelming majority of spectra contain line structures. Really interpreted quantities are the positions of maxima in emission spectra and minima in absorption spectra. Interpretation of these quantities provides the most reliable tool for the elucidation of the nature of a phenomenon being observed.

The present review proceeds from the concept of periodicity of meteorological parameters [4, 5]. Based on this concept, we distinguish specific properties of the spectrum of a purely periodic process and verify them using concrete

examples. It is natural to describe the presence of such properties as a *criterion for the existence of a spectral line*.

Furthermore, we compare the positions of lines in the spectra of variations of different physical characteristics, e.g. the spectral peaks of the atmospheric-pressure and sea-level variations. The occurrence of lines at identical frequencies suggests their similar origin.

The next step is to examine oscillation-induced phenomena. For example, purely periodic variations in the atmospheric pressure with a period of several weeks must give rise to a fine structure in the daily peak of temperature fluctuations. Such a fine structure is a line at a combination frequency equal to the sum of the diurnal-variation frequency and the frequency of the observed atmospheric-pressure variation. The presence of such a line confirms the reality of this variation.

The validity of the concept of periodicity of meteorological parameters is confirmed by concrete examples. Three of them are considered in this review. One ensues from the study of atmospheric-temperature variations associated with solar eclipses. An eclipse is a complex oscillatory process, the spectrum of which has a line structure. The coincidence of the observed lines with the eclipse spectral lines, together with the coincidence of the estimated line intensities, also testify to the reality of the periodic processes described below. Another example is given by a study of the fine line structure of the spectra of sea-level fluctuations with the period of the Moon's revolution around the Earth. The fine structure arises as a result of the frequency modulation of variations in the distance between the Earth and the Moon caused by the gravitational action of the Sun. It accounts for the characteristic line splitting and the appearance of additional intense lines, which are combinations of radial-oscillation frequencies with the frequency of the Earth's revolution around the Sun. The third example is the modulation of the solar irradiance by variations in the Earth's position relative to an elliptical orbit under the action of Jupiter and Venus. These phenomena have never been reported previously because of the low frequency resolution in the computation of meteorological-parameter spectra [6]. It is worth noting an analogy between the concept being developed in this paper and the theory of tides [7].

We believe that the above arguments collectively provide sufficient evidence for the reality of the line structure of atmospheric temperature- and pressure-variation spectra and make it possible to use this property for the solution of the important problem of long-term weather and climate forecasting. The fact is that such a structure with very narrow spectral lines contains a large share of the 'mathematical' energy of real variations, and a forecast based on the preliminary calculation of line parameters remains virtually unfailing for approximately 4 years in weather prediction and for 20 years in the case of predicting climatic changes. The significance of these predictions is in their practical implications. Retrospective illustrations of such forecasts are presented in this review.

The work is based on the construction of Fourier spectra using a discrete data set (periodograms). Well-developed numerical methods and software are available for the relevant calculations [8, 9]. The texts of the codes and analyses of possible mistakes can be found in the literature [10]. Also, the codes are included in the well-known software packages for data processing, such as MAPLE 6 [11], MATHLAB [12], and MATHEMATICA 4 [13].

2. Criterion for the existence of spectral lines

2.1 Coherence criterion

This section is devoted to the discussion of the possibility of observing a line structure in a spectrum while analyzing time series defined on a discrete sequence of points. Optimal methods for spectral maxima and minima analyses remain to be developed. According to the main idea of the interpretation of the information contained in a time series $y(t)$ [14], the phase and the frequency of oscillations are the quantities to be evaluated in the case of a periodic process, while the optimal observation statistic containing all relevant information is the spectrum

$$Sy(\omega) = \left| \int_0^T y(t) \exp(\mathrm{i}\omega t)\, \mathrm{d}t \right|^2 \qquad (1)$$

(T is the total observation time); estimates for the frequency ω and phase are the location of the maximum and the spectrum phase at the maximum, respectively [14].

A random process, for an optimal spectral-density evaluation [15], has to be divided into several (N) independent realizations of length T_1 (T/N); for each of them, the square of the spectrum is found as

$$Si(\omega) = \left| \int_{(i-1)\,T_1}^{i\,T_1} y(t) \exp(\mathrm{i}\omega t)\, \mathrm{d}t \right|^2 .$$

The optimal estimate is

$$A = \frac{1}{T} \sum Si . \qquad (2)$$

The accuracy of the estimate depends on the number of independent realizations N and increases with increasing N. A good accuracy can be achieved at $N > 10$. In this case, the frequency resolution $\delta\omega$ is significantly lower:

$$\delta\omega = \frac{\pi}{T_1} = \frac{\pi N}{T} .$$

An estimate of the spectral power is used in meteorological studies, commonly being referred to as the spectrum. The spectrum calculated in the present work is considered to be the observed periodicity statistic and is estimated with the use of (1). The spectrum value is essentially dependent on the length of the observation period T. In the case of a purely periodic process, the amplitude of the square at large T increases with increasing length of observation as T^2. In the case of a random process, the spectrum value also grows with T, but this growth is much slower, $\propto T$. An analysis of the duration dependence of the peak value can help us to differentiate between periodic components and spectral-density maxima of a random signal. It will be used below as a verification criterion for periodicity (coherence).

In what follows, this criterion will be illustrated by observations of the seasonal variations of meteorological parameters (coherent fluctuations with a period of 1 year and higher harmonics of this period). The criterion is used to verify the coherence of meteorological fluctuations with periods related to the Moon's revolution. Such fluctuations are known to influence the sea level [16], but they failed to be associated with variations in the atmospheric pressure and temperature.

Variations in the atmospheric pressure and temperature recorded at point Terneĭ (45.1°N, 136.5°E) and sea-level variations measured at point Kholmsk (47.0°N, 142.0°E) were used as observational materials.

2.2 Verification of the criterion through reliably interpreted maxima

The possibility of using the dependence of the spectral-line amplitude on the duration of observations as a criterion for distinguishing between coherent and incoherent spectral maxima is illustrated here by variations in the atmospheric pressure with a period of 1 year. This maximum describes the known coherent seasonal variations of the atmospheric pressure.

Observations made at point Terneĭ from 1966 to 1984 are used here by way of example. The observations are represented as a series of consecutive values with a 3-h cadence. In calculating the spectrum in the vicinity of a 1-year period, these data served as a source of daily values. The effect of the termination of the series was eliminated by preliminarily subtracting the result of smoothing over a 700-day interval from the daily values. Spectra were calculated for intervals of 1 year (1966), 2 years (1966–1967), 4 years (1966–1969), 6 years (1966–1961), 8 years (1966–1973), 10 years (1966–1976), 12 years (1966–1977), 14, 16, and 18 years. The data were taken at different frequency intervals. Figure 1a shows the results of calculations at a frequency interval of $\pi/500$ day^{-1}.

There is an apparent maximum in the vicinity of a 1-year period the amplitude of which displays a strong dependence on the duration of observations T. This dependence is shown in Fig. 1c (line *2*). The lines of coherent and incoherent origin have different slopes, as can be seen from lines R and C for the incoherent and coherent cases, respectively. Evidently, in both cases, line *2* markedly deviates from the theoretical predictions. The position of the maximum changes with increasing length of the observation period; a jump of the amplitude occurs at a period of 8 years. This feature of calculations — the nonmonotonic dependence of the spectral amplitude on the observation period — is encountered rather frequently and gives reason to regard a maximum as a random element. In fact, this is an immediate consequence of the use of insufficiently detailed data. The true period falls on an intermediate point. To illustrate this situation, the same spectra were calculated with an increased frequency resolution $\delta\omega$ (line *1*) using values $\delta\omega = \pi/2000$ and $\delta\omega = \pi/4000$. The dependences of the maximum amplitude on the duration of observations are shown in Fig. 1c. In the given situation, the maximum position is stable and the dependences are virtually identical in both cases; virtually, they are in perfect agreement with the theoretical dependence for the line of coherent origin.

Thus, sufficiently detailed data, with a sufficiently high frequency resolution, are needed to reveal the line structure of the spectrum. The limiting estimate for the resolution is $\delta\omega = \pi/T$. However, it follows from our calculations that even a lower resolution normally suits the purpose. It is important that the quantity be derived at a frequency close enough to the true one. The maximum is considered to be identified correctly if its location is T-independent at sufficiently large T and the amplitude increases rapidly enough. In fact, periodicity can be detected in the present case if the observation period is as short as 4 years.

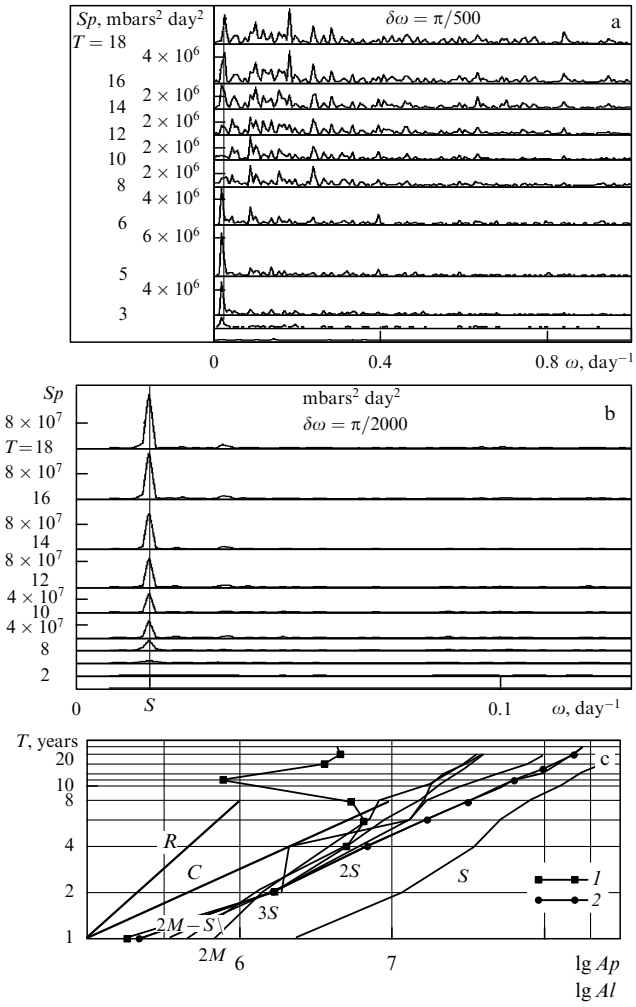

Figure 1. Spectra of atmospheric pressure at point Terneĭ, *Sp*, constructed from observations of different length T with a frequency resolution of (a) 0.00628 day^{-1} and (b) 0.00157 day^{-1}. The length T is indicated near the corresponding line. The frequency ω is in day^{-1}. (c) T-dependence of the spectral-maximum amplitude Ap for variations of atmospheric pressure during 1 year at different frequency resolutions: *1*, resolution 0.00157; *2*, resolution 0.00628. T-dependence of the spectral-maximum amplitude Al for sea-level variations: the maxima correspond to the periods of 1 year (S), 0.5 year ($2S$), 0.333 year ($3S$), 13.66 days ($2M$), and 14.17 days ($2M - S$). Lines C and R show slopes of the dependences for coherent and incoherent spectra.

Another example of well-studied coherent phenomena is provided by sea-level variations with a period of 1 year and with the lunar period of revolution around the Earth [16]. The data obtained at point Kholmsk (Sea of Japan) from 1951 to 1990 were used. They were taken at an interval of 12 h, and daily mean values were calculated. The series of daily values was smoothed over a 700-day interval, and the result was subtracted from the original series. The differences were used to compute the spectrum. The values were derived at an interval of $\delta\omega = \pi/2000$ day^{-1}. The spectra were calculated for periods of 1 year (1951), 2 years (1951–1952), 4 years (1951–1955), 6 years (1951–1956), 8 years (1951–1958), 10 years (1951–1960), 12 years (1951–1962), 14 and 16 years. The results were used to find the locations and amplitudes of unambiguously identifiable main maxima. These maxima occurred at frequencies S (1-year period), $2S$ (0.5-year period), $3S$ (1/3-year period), $2M$ (13.66-day period,

Table 1. Parameters of the main maxima in the spectrum of sea level variations at point Kholmsk.

	S		$2S$		$3S$		$2M$		$2M-S$	
year	day	$cm^2\,day^2$	day	$cm^2\,day^2$	day	$cm^2\,day^2$	day	$cm^2\,day^2$	day	$cm^2\,day^2$
1	381	2.3×10^6			117	6.9×10^5	13.5	3.4×10^5	14.3	4.5×10^5
2	381	1.2×10^7	210	1.9×10^6	125	1.4×10^6	13.6	1.6×10^6	14.2	1.3×10^6
4	381	3.5×10^7	186	2.1×10^6	121	3.9×10^6	13.6	6.2×10^6	14.2	5.0×10^6
6	364	5.2×10^7	182	1.3×10^7	121	7.3×10^6	13.65	1.3×10^7	14.2	9.1×10^6
8	364	7.9×10^7	182	1.7×10^7	121	8.2×10^6	13.65	1.6×10^7	14.2	1.5×10^7
10	364	1.3×10^8	182	2.8×10^7	121	1.7×10^7	13.65	1.8×10^7	14.2	2.0×10^7
12	364	1.7×10^8	182	4.8×10^7	121	2.2×10^7	13.65	2.2×10^7	14.2	2.7×10^7
14	364	2.3×10^8	182	7.4×10^7	121	3.0×10^7	13.65	3.1×10^7	14.2	3.3×10^7
16	364	2.9×10^8	182	1.0×10^8	121	3.6×10^7	13.65	3.9×10^7	14.2	4.0×10^7

or half the tropical month), and $2M - S$ (14.17-day period, a combination of the first harmonic of lunar revolution with seasonal variations). The maxima are clearly resolvable if the observation periods exceed 2 years. The parameters of the maxima, i.e. the period in days and the amplitude in $cm^2\,day^2$, are presented in Table 1. The length of the observation period in years is given in the first column.

The dependence of the amplitude on the length of the observation period is shown in Fig. 1c. By and large, it also coincides with the dependence $A \propto T^2$ predicted for a coherent case. The relations between the oscillation amplitudes at the frequency of the first lunar harmonic $2M$, the first harmonic of the first frequency of the Earth's revolution around the Sun $3S$, and the first negative combination of the first harmonic $2M$ with the frequency of the Earth's revolution around the Sun $2M - S$ are in reasonable agreement with the relations between the Newton tidal-potential amplitudes [7]. In calculation of daily values, the combination frequency appears in the Newton potential, as daily values are calculated, due to signal demodulation to the frequency of the Earth's diurnal rotation. Oscillations with a period of 1 year (S) and 1/3 year have been explained too [17] as resulting from the thermal expansion of water. Their amplitudes are proportional to the amplitudes of the first and third solar harmonics of atmospheric-pressure variations. The same phenomenon greatly contributes to the second-harmonic amplitude.

2.3 Spectral lines of sea level fluctuations at the frequency of the Moon's revolution

It can be seen from the analysis of the Newton tidal potential of lunar origin [7] that a maximum must also occur at the fundamental frequency (frequency of the Moon's revolution). The corresponding maximum is, however, ε^2 times smaller (ε is the lunar-orbit eccentricity). This maximum is described in the literature [16] and denoted as Mm. However, its observation in real spectra seems not quite convincing, unlike the case of the maxima considered in the preceding section. Figure 2a presents a portion of the spectrum in a frequency range from $2\pi/6$ to $2\pi/3$ day^{-1}. The spectrum was derived from the sea-level fluctuations recorded at point Kholmsk during 40 years, with a frequency resolution of 10^{-4} day^{-1}. A large number of maxima are well apparent, but only two of them (indicated by arrows) are included in the table in Ref. [16]. The detailed structure of the Mm maximum is shown in Fig. 2b. The main maximum occurs at the frequency of variations in the distance between the Moon and the Earth rather than at the frequency of the Moon's revolution, in agreement with Newton's theory [7]. The period of these fluctuations is 27.55 days; it is denoted by the special term *anomalistic month*. Figure 2a shows that this is neither the sole nor the main maximum in the frequency range under consideration. It is also interesting to examine some other observed maxima for coherence, e.g. those that occur at a combination of the Mm frequency and the fluctuations with a period of 0.5 year (frequency $2S$). The results of such a study are presented in Figs 2c and 2d. Figure 2c shows the sea-level-fluctuation spectra computed for different observation periods, with a frequency resolution increasing with the duration of observations. The maxima under consideration are denoted in Fig. 2c as $M - 2S$ and $M + 2S$. The corresponding frequencies are shown by straight lines. The lengths of the observation periods are indicated by Arabic numerals near the corresponding lines. The parameters of the maxima and the frequency resolution are presented in Table 2. The amplitude variations with the duration of observation are shown on a logarithmic scale in Fig. 2d.

Observations over a period of 12 years reveal an anomalous dependence, characteristic of estimates obtained with a low frequency resolution. Data for 14- and 16-year periods were recalculated with a higher resolution. However, this resolution still proves insufficient for longer observation periods. Therefore, the calculations were made with an additionally increased resolution.

The patterns of dependence on the length of the observation period give unambiguous evidence of coherence in the sea-level perturbation. Its amplitude is significantly larger than the expected one (in agreement with the theory of tides). The intensities of lines $M - 2S$ and $M + 2S$ are roughly equal and exceed those of lines $M - S$ and $M + S$, which can also be clearly observed. However, these are not the only lines in a cyclic-frequency range from 0.1 to 0.3 day^{-1}. Twenty four other lines can be unequivocally distinguished within this range. The corresponding periods are 1) 62.62, 2) 58.7, 3) 56.43, 4) 54.65, 5) 53.78, 6) 52.3, 7) 50.75, 8) 48.67, 9) 47.3, 10) 45.6, 11) 44.5, 12) 42.49, 13) 38.0, 14) 35.6, 15) 34.1, 16) 29.35, 17) 29.61, 18) 28.52, 19) 27.02, 20) 26.35, 21) 25.29, 22) 24.35, 23) 23.54, and 24) 22.91 days. These variations are coherent and observable throughout the entire 40-year period.

This means that the proposed criterion for distinguishing spectral lines that correspond to purely periodic processes is suitable for the analysis if supplemented by the requirement to use detailed data (sampling points). It is due to the insufficiently detailed analysis that anomalous dependences of the line amplitudes on the length of the observation period occur and discredit the line representation of the spectrum. However, some anomalies are not related to the low frequency resolution, being attributable to the fine structure of the corresponding peaks, quite apparent in Fig. 2b. It can

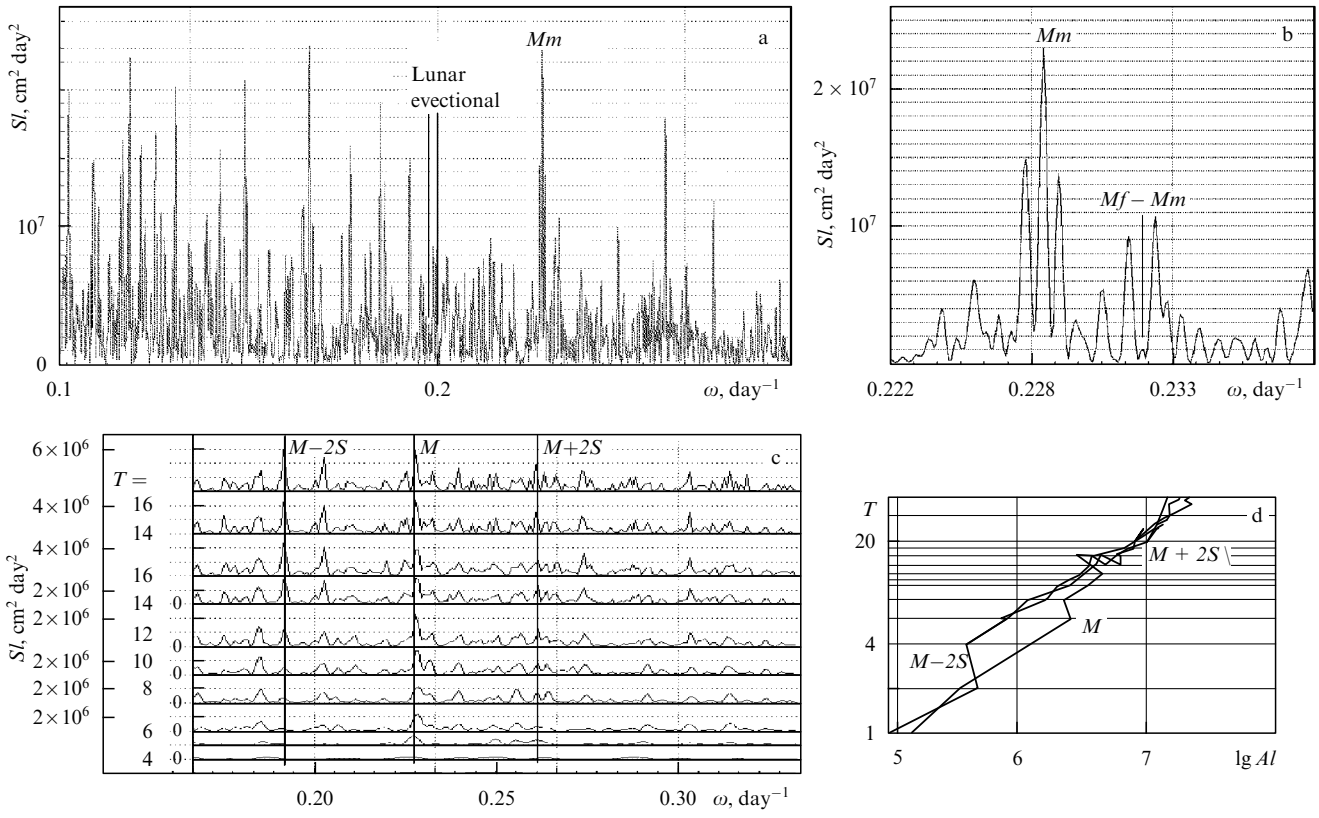

Figure 2. (a) Spectra of sea-level variations at point Kholmsk, *Sl*: (a, b) for 1950 – 1990; frequency ω is in day^{-1} [the vicinity of the *Mm* maximum is shown (b)]; (c) at different durations of observation T in the vicinity of the lunar revolution frequency M; frequency ω is in day^{-1}; T (years) is indicated near the corresponding line; (d) the spectral-maximum amplitude Al at frequencies M, $M-2S$, $M+2S$ versus the observation period T in years.

be seen that the *Mm* peak is split into three lines spaced at approximately 6×10^{-4} day^{-1}. Such a splitting becomes noticeable in the spectra when the observation period is about 10 years, with the main peak amplitude undergoing a 2-fold stepwise decrease. This anomaly is clearly represented in Fig. 2d.

Table 2. Parameters of the maxima in the spectra of sea-level variations at the lunar revolution frequency M and at the frequency combinations $M - 2S$ and $M + 2S$.

Observation interval (years)	Parameters of line $M-2S$: period (days), amplitude (cm^2 day^2)		Parameters of line M: period (days), amplitude (cm^2 day^2)		Parameters of line $M+2S$: period (days), amplitude (cm^2 day^2)		Resolution (day^{-1})
1	34	1.13×10^5	27.39	1.54×10^5			7.84×10^{-4}
2	33.6	3.1×10^5	27.7	3.6×10^5			
4	33.7	4.9×10^5	27.58	1.3×10^6		10^5	
6	32.9	4.1×10^5	27.49	2.58×10^6	24.02	7.4×10^5	
8	32.78	8.3×10^5	27.49	2.3×10^6	24.02	1.68×10^6	
10	32.78	1.2×10^6	27.49	3.43×10^6	24.02	2.04×10^6	
12	32.78	2.5×10^6	27.58	4.53×10^6	24.02	3.13×10^6	
14	32.78	3.3×10^6	27.49	3.68×10^6	24.02	3.68×10^6	
16	32.78	4.1×10^6	27.49	3.78×10^6	24.02	2.9×10^6	
14	32.41	4.5×10^6	27.49	4.83×10^6	24.04	3.68×10^6	3.92×10^{-4}
16	32.75	6.3×10^6	27.49	5.85×10^6	24.04	3.8×10^6	
16	32.68	4.7×10^6	27.51	5.85×10^6	24.06	3.96×10^6	1.96×10^{-4}
18	32.68	5.6×10^6	27.51	7.27×10^6	24.06	6.6×10^6	
20	32.68	7.98×10^6	27.51	1.01×10^7	24.05	8.2×10^6	
24	32.68	1.14×10^7	27.51	1.21×10^7	24.04	9.5×10^6	
20	32.68	7.98×10^6	27.51	1.02×10^7	24.05	8.0×10^6	9.8×10^{-5}
26	32.68	1.35×10^7	27.51	1.2×10^7	24.04	1.14×10^7	
28	32.66	1.24×10^7	27.51	1.44×10^7	24.05	1.28×10^7	
30	32.68	1.28×10^7	27.53	1.53×10^7	24.04	1.56×10^7	
36	32.66	1.41×10^7	27.55	2.24×10^7	24.04	1.49×10^7	
38	32.68	1.43×10^7	27.55	1.98×10^7	24.04	1.78×10^7	
40	32.68	1.48×10^7	27.55	2.29×10^7	24.05	1.84×10^7	

3. Comparisons between the lines in the spectra of meteorological parameter variations

3.1 Spectral lines of atmospheric pressure, air temperature, and sea level in the range from 62 to 20 days

Comparisons of spectral amplitudes of atmospheric pressure and sea-level fluctuations are used in investigations into the nature of variations [39]. The principal question is whether they are generated in the air or in the ocean. Identification of individual lines permits one to address this question in a more detailed and accurate manner because ordinary, strongly smoothed spectra are calculated based on the analysis of mixed data containing several lines of different nature. The very fact of the appearance of spectral maxima of the variations of different parameters at the same frequency confirms the physical reality of these maxima. This fact will be illustrated below by the spectra of variations in the sea level, atmospheric pressure, and air temperature in a range from 63 to 20 days. The spectra were constructed based on formula (1) using the data on the atmospheric pressure and temperature obtained at point Terneĭ in 1966 – 1984 and the data on sea-level fluctuations at point Kholmsk in 1951 – 1990. For this range of periods of sea-level fluctuations, only the lines corresponding to the period of variations in the distance between the Moon and the Earth (*Mm*, $T = 27.55$ days) and lunar evectional period ($T = 31.812$ days) have been discussed in the literature [16, 7]. Other interesting maxima (Fig. 2a) remain to be described. The source of these deterministic events is unknown.

Daily values were derived from observations represented at 3-h intervals. Thereafter, the spectrum was constructed following the same procedure as in the evaluation of sea-level fluctuation spectra. These spectra were compared in Fig. 3a. The spectra were obtained with a frequency resolution of $\delta\omega = 10^{-4}$ day^{-1}. Like the spectra of sea-level fluctuations (graph *3*), the temperature (graph *1*) and pressure (graph *2*) spectra exhibit many peaks that can be collectively interpreted as a line structure. Some of these maxima coincide in their position, to a certain degree of accuracy, with spectral lines of sea-level fluctuations. The characteristics of these maxima (period and amplitude) are presented in Table 3. The table, compared to the above list of spectral lines of sea-level fluctuations, includes additional lines, since they are well pronounced in the pressure variation spectra. The line numbers are given in the first column, the periods and intensities of the spectral lines of sea-level fluctuations in the second and third columns, the same parameters of atmospheric pressure fluctuations in the fourth and fifth columns, and the parameters of air-temperature fluctuations in the

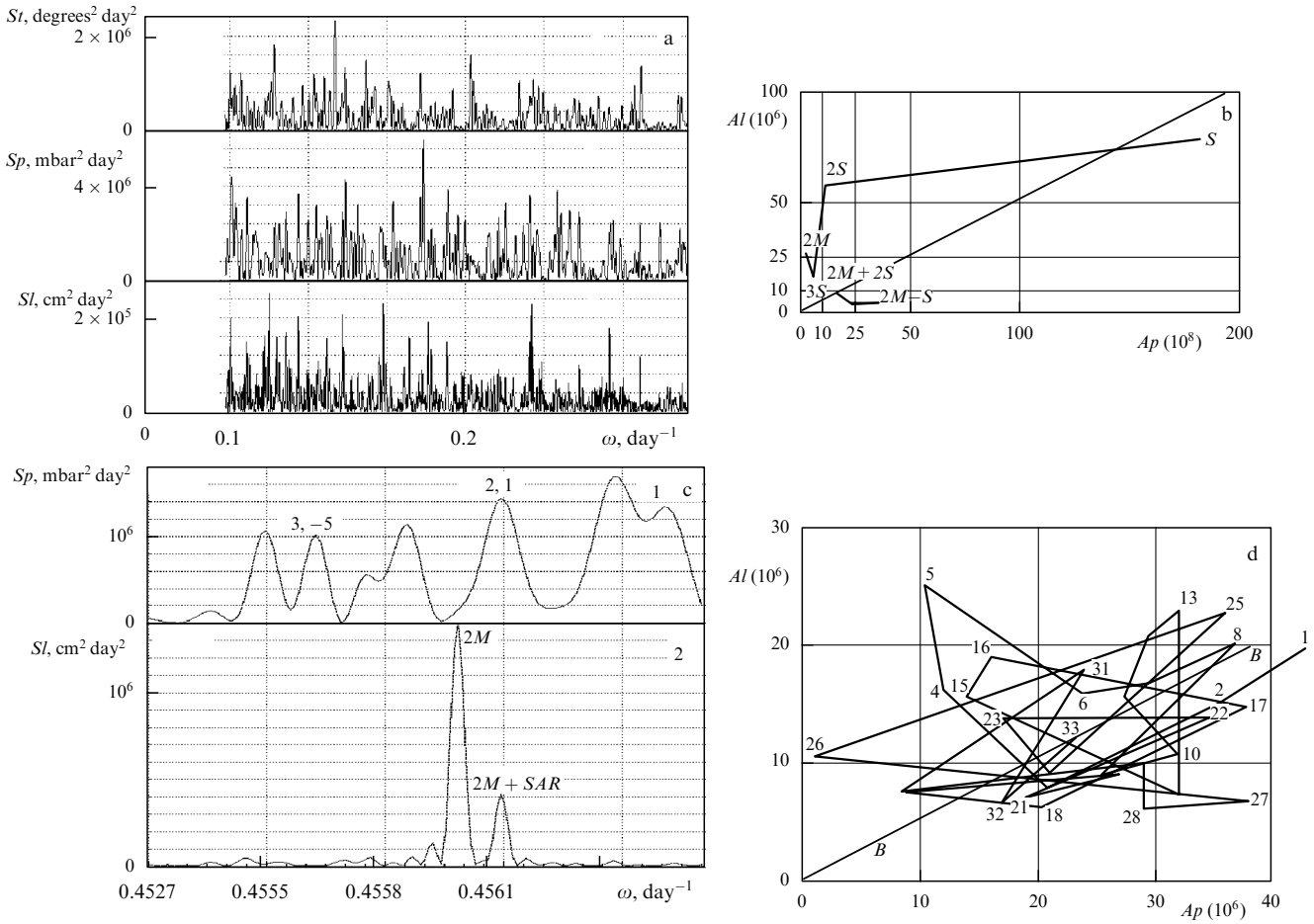

Figure 3. (a) Spectra of fluctuations in the air temperature (*ST*), atmospheric pressure (*Sp*), and sea level (*Sl*) in the range from 62 to 20 days. (b) Relationship between the spectral-line amplitudes of atmospheric pressure (*Ap*) and sea-level fluctuations (*Al*). (c) Fine structure of line 2*M* in the spectra of atmospheric pressure (*Sp*) and sea-level fluctuations (*Sl*). Frequency ω is in day^{-1}. (d) Relationship between the amplitudes of corresponding spectral lines of atmospheric-pressure (*Ap*) and sea-level (*Al*) fluctuations. Line *B* represents the inverted barometric law. Line numbers correspond to those in Table 3.

Table 3. Parameters of lines in the spectra of sea-level, atmospheric-pressure, and air-temperature fluctuations.

No	Sea level		Atmospheric pressure		Temperature	
	Period (days)	Amplitude ($cm^2\,day^2$)	Period (days)	Amplitude ($mbar^2\,day^2$)	Period (days)	Amplitude ($degrees^2\,day^2$)
1	62.62	1.98×10^5	62.43	4.28×10^6	62.74	1.26×10^6
2	58.7	1.48×10^5	58.7	3.48×10^6	58.55	7.3×10^5
3	56.43	8.01×10^4	56.43	2.08×10^6	—	4.7×10^5
4	54.65	1.63×10^5	54.65	1.2×10^6	54.65	6.9×10^5
5	53.78	2.52×10^5	—	1.03×10^6	53.91	7.6×10^5
6	52.3	1.59×10^5	52.67	2.38×10^6	52.78	1.8×10^6
7	50.75	1.69×10^5	50.75	2.95×10^6	—	3.2×10^5
8	48.67	2.02×10^5	48.67	3.69×10^6	—	8.87×10^5
9	47.3	8.89×10^4	47.19	2.54×10^6	—	7.2×10^5
10	45.6	1.08×10^5	45.9	3.2×10^6	45.9	8.1×10^5
11	44.5	1.57×10^5	44.5	2.74×10^6	44.7	1.15×10^6
12	42.49	2.06×10^5	42.49	2.93×10^6	42.49	8.0×10^5
13	38.0	2.3×10^5	38.11	3.2×10^6	—	4.8×10^5
14	37.20	7.2×10^4	37.10	3.2×10^6	—	6.4×10^5
15	35.6	1.56×10^5	35.6	1.4×10^6	—	1.5×10^5
16	34.09	1.90×10^5	34.09	1.6×10^5	—	5.1×10^5
17	32.66	1.48×10^5	32.63	3.8×10^6	32.27	8.0×10^5
	32.06	5.8×10^4	31.90	1.3×10^5	32.01	10^4
18	29.89	6.23×10^4	29.89	2.03×10^6	30	3.91×10^5
19	29.61	7.6×10^4	29.61	8.9×10^5	—	3.1×10^5
20	29.35	9.1×10^4	29.35	2.7×10^6	—	1.0×10^5
21	28.52	7.2×10^4	28.45	1.9×10^6	28.19	1.1×10^6
22	27.64	1.4×10^5	27.59	3.47×10^6	27.59	7.2×10^6
23	27.46	1.38×10^5	27.46	1.7×10^6	27.46	1.0×10^6
24	27.153	9.2×10^4	27.21	2.1×10^6	27.24	9.5×10^5
25	27.55	2.29×10^5	*Mm*			
26	27.02	1.06×10^5	—	9.0×10^6	26.94	8.4×10^7
27	26.35	6.8×10^4	26.30	3.8×10^6	26.35	5.0×10^5
28	25.75	6.1×10^4	25.56	2.9×10^6	25.71	4.0×10^5
29	25.29	9.9×10^4	25.29	2.9×10^6	25.30	6.4×10^5
30	24.35	7.5×10^4	24.32	8.4×10^6	24.32	3.9×10^5
31	24.03	1.80×10^5	24.06	2.4×10^6	24.06	4.9×10^5
32	23.54	6.79×10^4		1.7×10^6		5.3×10^5
33	22.91	1.19×10^5	22.91	2.3×10^6	22.88	1.4×10^6

sixth and seventh columns. Amplitudes of sea-level, atmospheric-pressure, and temperature fluctuations are expressed in $cm^2\,day^2$, $mbar^2\,day^2$, and $degree^2\,day^2$, respectively.

The spectrum of sea-level fluctuations is based on the 40-year period, and the spectra of atmospheric pressure and temperature on the 19-year period. The spectral lines are more pronounced in the spectrum of sea-level fluctuations. In the spectra of the atmospheric pressure and air temperature those lines can mainly be distinguished that correspond to maxima in the sea-level fluctuation spectrum. The majority of the lines have counterparts in the spectrum of atmospheric-pressure fluctuations. However, not all of the observed atmospheric-pressure lines are among such counterparts. For example, a well-defined line in the spectrum of pressure variations with a period of 34.46 days and an amplitude of 5.99×10^6 corresponds to a rather weak line in the sea-level fluctuation spectrum ($T = 34.57$ days, $A = 8.8 \times 10^4$). Similarly, the strongest line in the spectrum of temperature variations ($T = 43.4$ days, $A = 2.33 \times 10^6$) proved to have no analog in the spectrum of sea-level fluctuations.

Another line that does not appear in the table is a strong line in the air-temperature spectrum corresponding to a maximum in the spectrum of pressure variations. It has a period of 34.68 days and an amplitude of 1.18×10^6.

With few exceptions, the periods of lines do not coincide exactly. The differences may cover a few sampling points and are absolutely reliable. They persist if the spectra of sea-level fluctuations are calculated for a period of 20 years. As a rule, they are greater than the variations in the line location due to changes in the observation period within a range from 18 to 40 years, shown in Table 2. The lines have a fine structure that can be well resolved using the adopted computational scheme. An example of such a fine structure for line *Mm* in the spectrum of sea-level fluctuations is presented in Fig. 2b. There is no doubt, however, that spectra of air-temperature, atmospheric-pressure, and sea-level fluctuations contain sharp lines at identical frequencies.

3.2 Comparisons between the spectral amplitudes of different meteorological parameters

Comparisons between the spectral amplitudes of different meteorological parameters are conducive to the elucidation of mechanisms of action of various factors on weather conditions. Line frequency is normally a reliable indicator of the source of a perturbation. Relative values of spectral amplitudes subject to marked variations can be used to identify the mechanisms underlying the generation of the variations. For example, if variations are generated in the atmosphere, the horizontal gradients of atmospheric-pressure variations Δp_a give rise to compensatory horizontal gradients of sea-level fluctuations ζ_a, and the amplitudes of these variations are related by the so-called inverted barometric law [7], $\rho_1 g \zeta_a = \Delta p_a$, where ρ_1 is the water density. Conversely, sea-level fluctuations ζ_0 cause air movement over the water

surface and thus lead to changes in the atmospheric pressure Δp_0. The amplitudes of these fluctuations are related by the equality $\rho_0 g\zeta_0 = \Delta p_0$, where ρ_0 is the air density. This means that the variations of the atmospheric pressure in the latter case are three orders of magnitude smaller than in the former. A similar difference occurs when the variations generated in one medium are recorded in the other. In this case, a wave traveling in the atmosphere with an amplitude of Δp_{a1} (waves with periods in excess of 24 hours are referred to as *Rossby waves, or planetary waves* [18]) induces a concomitant wave in the ocean with the amplitude of level variations

$$\zeta_{a1} = \frac{\Delta p_{a1}}{(\rho_1 g)} \frac{H_2}{H_1 - H_2} .$$

The wave propagating in the ocean with an amplitude of ζ_{01} generates a wave in the atmosphere with the pressure-variation amplitude [18]

$$\Delta p_{01} = (\rho_0 g) \frac{H_2}{H_1 - H_2} \zeta_{01} .$$

Therefore, if variations are generated in the ocean, the ratio of the amplitude of the atmospheric-pressure spectrum to the amplitude of sea-level fluctuations is also approximately 1000 times smaller. In the above formulas, H_2 is the ocean depth and $H_1 = 7800$ m [7] is the scale height of the atmosphere. The formulas were derived using a model of long-wave propagation in a two-layered medium within a rotating coordinate system, placed in a gravity field [18], in the absence of mass exchange between the two media. In this model, the variations η_1 and η_2 of the upper and lower layer surfaces, respectively, were used to characterize waves, while the densities ρ_0 and ρ_1 and thicknesses H_1 and H_2 were characteristics of the upper and lower layers. Both the Coriolis force (parameter f) and the force of gravity were taken into consideration. The upper medium served to simulate the atmosphere ($\rho_0 = 0.00129$ g cm^{-3} and $H_1 = 7900$ m) and the lower one, to simulate the ocean ($\rho_1 = 1.0$ g cm^{-3} and $H_1 = 5000$ m). Fluctuations of the sea level were coincident with η_2, and the variations of pressure with $g\rho_0\eta_1$. In this model, there were two modes of traveling waves in which the variations η_1 and η_2 were related by the equalities $\eta_{1a} = -q_a\eta_{2a}$ and $\eta_{10} = -q_0\eta_{20}$, while the quantities q_a and q_0 were the roots of the equation

$$\frac{\rho_0}{\rho_1} H_2 q^2 + \left(H_1 - H_2 + 2H_2 \frac{\rho_0}{\rho_1}\right) q - H_2\left(1 - \frac{\rho_0}{\rho_1}\right) = 0 . \quad (3)$$

In the case under consideration, $\rho_0/\rho_1 \ll 1$ and one of the solutions to (3) is large and equals $q_a = -(\rho_1/\rho_0)[(H_1 - H_2)/H_2]$. It determines a relationship between the variation amplitudes for a wave propagating in the atmosphere. The second solution $q = H_2/(H_1 - H_2)$ does not depend on the density ratio. These relations between the spectral amplitudes can be specified by an analysis of the relationship between the amplitudes of spectral lines whose origin is known to a certain extent, which are excited by the Earth's revolution around the Sun and lunar revolution around the Earth. The spectra were constructed using sea-level fluctuations averaged over 48 hours for the period from 1951 to 1990 and similarly averaged variations of the atmospheric pressure during 1966 – 1984. The solar lines S, $2S$, $3S$ and lunar line $2M$ are most intense and readily distinguishable in the corresponding parts of the spectra. Their parameters are presented in Table 4.

The corresponding amplitudes are shown in Fig. 3b. Also shown is the line corresponding to the inverted barometric law. Strong (S, $2S$, $3S$, $2M$) and relatively weak lines are represented on different amplitude scales. Lines S and $2M$ are most interesting.

Line S (period 365.25 days) describing seasonal variations in the atmospheric pressure and sea level agrees fairly well with the inverted barometric law, although the amplitude of pressure variations is somewhat larger than expected. It is in best agreement with the amplitude ratio in a wave generated in the atmosphere of the two-layered model. The estimate of 1.24 obtained for the quantity $H_2/(H_1 - H_2)$ corresponds, at the adopted thickness of atmosphere, to a mean sea depth of 3500 m.

Line $2M$ (period 13.661 days) is denoted as Mf in the theory of tides. For this line, the amplitude of the spectrum of sea-level fluctuations is approximately 10 times that predicted by the inverted barometric law. On the one hand, this is unambiguous evidence for an oceanic origin of these fluctuations. On the other hand, in this case, the amplitude of the spectrum of atmospheric-pressure variations is 10^5 times larger than the amplitude of this line estimated in the theory of atmospheric tides [7, 19] and the amplitude of the atmospheric wave concomitant to the tidal waves. This latter amplitude is of special interest in the context of the theory of ocean – atmosphere interaction [3]. The striking discrepancy between the theoretical and experimental estimates calls for a more careful analysis of the problem. The action of the Moon on the ocean and atmosphere is not due to gravity alone. The next section will be devoted, inter alia, to the analysis of lunar action through the modulation of solar irradiance. Various mechanisms account for the appearance of a maximum at a

Table 4. Amplitudes of spectral lines of known origin.

Designation	Sea-level fluctuations		Pressure		Temperature	
	Period	Amplitude	Period	Amplitude	Period	Amplitude
S	365.71	7.89×10^6	365.71	1.823×10^8	365.71	2.46×10^9
$2S$	182.336	5.78×10^6	182.857	1.146×10^7	181.303	2.72×10^7
$3S$	121.673	1.624×10^6	122.84	5.8×10^6	121.90	8.26×10^6
$2M$	13.660	2.81×10^6	13.695	1.14×10^7	13.76	5.0×10^5
			13.631	1.43×10^7	13.65	3.6×10^7
$2M-S$	14.178	4.6×10^4	14.153	2.2×10^6	14.14	5.5×10^5
			14.26	3.57×10^6	14.25	8×10^5
$2M-2S$	14.76	4.0×10^4	14.72	2.35×10^6	14.72	1.9×10^6
$2M+S$	13.185	8.8×10^4	13.176	1.61×10^6	13.155	2.9×10^5
$2M+2S$	12.70	1.1×10^5	12.74	1.73×10^6	12.70	3.2×10^5

frequency close to but not identical with that of the $2M$ line. Different theories yield frequency shifts attributable to minor particularities in the Moon's motion, such as the difference between the revolution and radial-oscillation frequencies [difference between the tropical (27.321 days) and anomalistic (27.554 days) months] or the frequency of revolution (regression) of lunar orbital nodes (period 18.613 years). In order to differentiate such effects, the spectra should be analyzed with a high-frequency resolution using observations of a maximally long duration. Fine structures of the spectra of sea-level and atmospheric-pressure variations in the vicinity of the $2M$ frequency are compared in Fig. 3c. Graph *1* represents the spectrum of pressure variations and graph *2*, the spectrum of sea-level fluctuations. The source data were the same as before. The atmospheric pressure was recorded over 19 years and the sea-level fluctuations for 40 years. The frequency resolution was 10^{-4} day^{-1}. It can be seen that the spectrum of sea-level fluctuations contains not only the line Mf (period 13.661 days) but also a line at a frequency of $2M + \mathrm{SAR}$ (SAR is the regression frequency of the lunar orbital nodes). The spectrum of pressure variation contains four intense lines at frequencies shifted relative to $2M$ (against their tails, the line $2M$ is not distinguishable). It will be shown in the next section that lines 2,1 and 3, -5 are generated in the atmosphere as a result of solar-radiation modulation by lunar eclipses. Only a preliminary conclusion can be drawn with respect to the line associated with the concomitant tidal wave in the atmosphere. Namely, the spectral-line amplitude of the concomitant wave of oscillations excited in the ocean is no larger than 10^{-2} of the amplitude estimated from the inverted barometric law.

Combination lines either conform to the $2M - 2S$ law or reflect larger pressure variations compared to amplitude variations. It can be concluded that the inverted barometric law is satisfied if variations are generated by surface events. If the source of variations lies in the bulk of water (line $2M$), the sea-level fluctuations exceed the corresponding variations in the atmospheric pressure. It is worthwhile to note that combinations of the lunar harmonic with frequency S are not of tidal origin. It follows from the corresponding spectral-amplitude ratio that they are generated by the same mechanism as seasonal variations (S).

Figure 3d compares the spectral-line amplitudes of the atmospheric-pressure and sea-level fluctuations. Line numbers corresponding to those in Table 3 are placed at the respective points. The line depicting the inverted barometric law is shown separately. It can be seen that the majority of points agree with this law fairly well. For certain lines, the variations of the sea level substantially exceed the corresponding pressure variations. For others, the reverse is true.

Thus, the amplitude ratio of mutually corresponding spectral lines of atmospheric-pressure and sea-level fluctuations can be used to locate primary perturbations. Variations are primarily generated in the atmosphere or at the interface between the two media if their amplitudes obey the inverted barometric law or the spectral-line amplitude of atmospheric pressure is larger than that predicted from the measured sea-level fluctuation amplitude on the basis of the inverted barometric law. Otherwise, variations are generated in the bulk of water.

This line of reasoning leads to the inference that harmonics at frequencies $2M - 2S$, $2M - S$, $2M + S$, and $2M + 2S$ are generated in the atmosphere, being probably a consequence of the modulation of solar irradiance by the Moon's motion.

Thus, the spectra of variations in the atmospheric pressure, air temperature, and sea level with periods ranging from 20 to 60 days have a line structure. The periods of lines of variations in different parameters coincide with a fairly high accuracy, while the relative amplitudes of lines vary considerably. Nevertheless, the spectral lines of atmospheric-pressure and sea-level variations can be divided into two groups according to their relative amplitudes. For the lines of the first group, the amplitude ratio is close to 1 mbar^2 cm^{-2}. This group includes the well-known line of seasonal variations with a period of 1 year. In the second group, the amplitude ratio is close to 0.1 mbar^2 cm^{-2}. It includes the line with a period of 13.6 days excited by tidal fluctuations produced by the gravitational action of the Moon.

4. The origin of the periodic variations of sea level, atmospheric pressure, and air temperature in the range from 10 to 60 days

4.1 Introduction

One of the most convincing arguments in support of the physical reality of the observed periodic variations in the atmospheric pressure and temperature is the understanding of their origin. The Newtonian theory of tides [7] greatly promoted the acceptance of the idea of tidal periodicity. In what follows, we will discuss attempts to develop a theory explaining the role of the Moon in the variations of the air temperature, atmospheric pressure, and sea level. Solar radiation is supposed to be the principal factor responsible for variations in the atmospheric temperature and pressure. As in Newton's theory [7], the main factor that causes sea-level fluctuations is the gravitational action of the Moon. The kinematic parameters of lunar and solar motions are the basic parameters determining the positions of spectral lines of meteorological variations. Information about these motions has been collected by astronomers [20], while the location and structure of the lines can be found theoretically.

4.2 Tidal-wave generation in the ocean at the characteristic frequencies of lunar motion

Sea-level fluctuations generated in the ocean are described by an expression for the static level deviation ζ caused by the tidal wave of Newton's theory [7]:

$$\zeta = \frac{3}{2} H\left(\cos^2\Delta - \frac{1}{3}\right)\left(\cos^2\theta - \frac{1}{3}\right) + \frac{1}{2} H \sin 2\Delta \sin 2\theta \cos(\alpha + \varphi) + \frac{1}{2} H \sin^2\Delta \sin^2\theta \cos 2(\alpha + \varphi)\,. \quad (4)$$

In this formula, Δ is the angle between the directions toward the Moon and a pole, θ is the colatitude of the point of interest, α is the angle of the Earth's rotation about its axis, φ is the latitude of the observation point [1], $H = (3/2)(M/E)(a/D)^3 a$, a is the Earth's radius, D is the radius of the Moon's orbit, M and E are the masses of the Moon and the Earth, respectively (the same notation is used as in Ref. [7]).

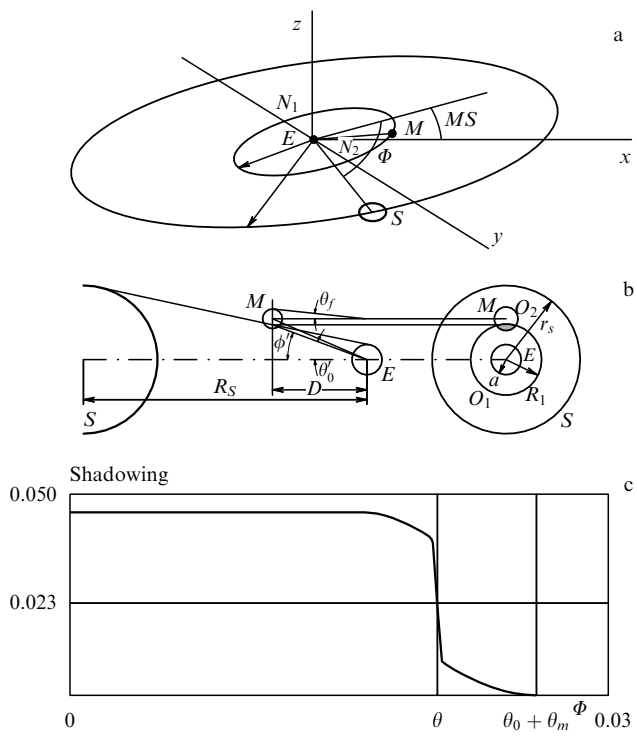

Figure 4. (a) System of coordinates. (b) Two projections of the positions of celestial bodies (*S* is the Sun; *E*, the Earth; *M*, the Moon); right: projection onto the plane perpendicular to the direction from the Earth to the Sun; left: projection onto the plane that passes through the centers of the Sun, Earth, and Moon. The effective shadowing area is shaded. (c) Dependence of Sun occultation by the Moon on the angle between the directions towards the Sun and the Moon.

Figure 4a is a schematic representation of the relative positions of celestial bodies, the trajectories of the Earth and Moon, the lunar orbital nodes N_1 and N_2, the coordinate axes associated with the Earth and used for calculations. In this coordinate system, axis z is perpendicular to the ecliptic plane (plane of the Earth's revolution around the Sun). Axis y coincides with the line of intersection of the Moon's orbit plane with the ecliptic plane. The origin coincides with the Earth's center. This system of coordinates rotates in space about the z axis with the frequency of 'regression of lunar orbital nodes'

$$\omega_4 = \frac{2\pi}{6585.32} = 9.54 \times 10^{-4}\ \text{day}^{-1}.$$

In this coordinate system, the Sun revolves around the Earth at a frequency of $\omega_2 + \omega_4$ in plane xy, while the Moon orbits the Earth with the frequency $\omega_1 + \omega_4 \cos MS$;

$$\omega_2 = \frac{2\pi}{365.25} = 1.7 \times 10^{-2}\ \text{day}^{-1},$$

$$\omega_1 = \frac{2\pi}{27.321} = 0.230\ \text{day}^{-1}.$$

The quantity MS is $5°8'43''$ [5], $\cos MS = 0.9962$, which differs from unity only slightly, and this difference can be neglected in further calculations. In the system under consideration, the coordinates of the Moon (Mi) and the Sun (Si) are written as

$$Mz = D \sin MS \cos(\omega_1 + \omega_4)\, t,$$
$$My = D \sin(\omega_1 + \omega_4)\, t,$$
$$Mx = D \cos MS \cos(\omega_1 + \omega_4)\, t,$$
$$Sz = 0,$$
$$Sy = Rs \sin(\omega_2 + \omega_4)\, t,$$
$$Sx = Rs \cos(\omega_2 + \omega_4)\, t.$$

The cosine of the angle Φ determining the lunar phase is

$$\cos\Phi = \cos MS \cdot \cos(\omega_1 + \omega_4)\, t \cdot \cos(\omega_2 + \omega_4)\, t + \sin(\omega_1 + \omega_4)\, t \cdot \sin(\omega_2 + \omega_4)\, t. \quad (5)$$

In these formulas, the time t is measured from New Moon and Rs is the radius of the Earth's orbit. The Moon's orbital plane intersects the plane xy along axis y. The equation of this plane is

$$z \cos EM = x \sin EM,$$

where EM is the angle between the equatorial plane and the lunar orbital plane. The direction from the center toward the Moon lies in this plane and makes an angle α with the line $y = 0$; $z \cos EM = x \sin EM$. Angle φ is measured from the Greenwich meridian and time t from the moment at which the direction toward the Moon comes to lie in plane xz. In this case,

$$\alpha + \varphi = (\omega_0 - \omega_1 - \omega_2)\, t;$$

where $\omega_0 = 2\pi$ day^{-1} is the frequency of the Earth's rotation about its axis. The first correction arises as a result of the change in the direction toward the Moon, and the second one is due to the Earth's revolution around the Sun the phase of which is used for the evaluation of the rotation period. The quantity Δ is well known. It has frequently been estimated in analyses of tides:

$$\cos\Delta = \sin EM \cdot \cos\omega_1 t. \quad (6)$$

The angle EM can be found in astronomical year-books [21]. It varies from $18°18'$ to $28°35'$ with the of 18.613-year (6585-day) period of lunar-node regression [22]. Its maximum values fell on August 1950, March 1969, and November 1988 [22]. The variation of the sine of this angle with time can be described by the equation

$$\sin EM = \sin E \cdot \cos MS + \cos E \cdot \sin MS \cdot \cos\omega_4 t. \quad (7)$$

Here, $E = 23°33'$ is the inclination of the Earth's orbit.

Only low-frequency spectral maxima will be analyzed below. Therefore, only the first term is sufficient to consider in formula (4):

$$\zeta_1 = \frac{3}{2} H \left(\sin^2 EM \cdot \cos^2 \omega_1 t - \frac{1}{3} \right) \left(\cos^2\theta - \frac{1}{3} \right). \quad (8)$$

In order to describe the main lines related to the Moon's motion, the time dependence of H must be taken into account. Additional lines appear as a result of the time dependence of the distance between D and the Moon. It is usually assumed that the Moon moves relative to the Earth in an elliptic orbit with a small eccentricity $e = 0.055$ [22]. However, the period of variations in the distance between

the Moon and the Earth (the anomalistic month equal to 27.555 days) does not coincide with the period of revolution. The discrepancy is large enough to be noticeable in the analysis of a series of observations for a period over 10 years. In this case, the distance D can be found from the equation

$$\frac{P}{D} = (1 + e\cos\omega_3 t)\,; \tag{9}$$

where P in the parameter of the orbit, $\omega_3 = 2\pi/27.555$, and $H \propto D^{-3}$.

The expression for the tidal potential contains purely periodic functions with three frequencies $2\omega_1$, ω_3, ω_4. Its spectrum contains three lines that are combinations of these three frequencies: $\omega_{i,j,k} = i\,2\omega_1 + j\,\omega_3 + k\,\omega_4$ (i, j, k are integers). However, these combinations differ in intensity. The expression contains small parameters. The parameter $\cos E \cdot \sin MS = 0.0752$ appears as a multiplier each time when the combination includes the frequency ω_4, and the parameter $e = 0.055$ when the combination contains the frequency ω_3. Moreover, the frequency $2\omega_1$ appears as a purely sinusoidal factor, i.e. the quantity i assumes only three values: -1, 0, and 1. In this case, the main components correspond to frequencies 0 ($i = 0$, $j = 0$, $k = 0$) and $2\omega_1$ ($i = \pm 1$, $j = 0, k = 0$). The latter is the known line M_f [16]; the spectrum of sea-level fluctuations in the vicinity of this line is shown in Fig. 3c. This spectrum also contains two more lines ($i = \pm 1$, $j = 0$, $k = \pm 1$). Their relative intensity is in good agreement with the theoretical estimate in the case of the line ($i = 1$, $j = 0$, $k = -1$) and approximately 10 times higher in the case of the line ($i = 1$, $j = 0, k = 1$).

Lines at frequencies ω_3 ($i = 0$, $j = 0$, $k = 1$) and $2\omega_1 - \omega_3$ ($i = 1, j = -1, k = 0$) are next in terms of intensity. The first of them, Mm, is shown in Fig. 2b, where the second one can be seen too. In order to make them distinguishable, the figure also presents theoretical spectral lines (Mm and $Mf - Mm$). In the case under consideration, the lines are difficult to distinguish, they have a specific shape lacking in the theoretical representation. Line Mm splits into three and line $Mf - Mm$ into four components. This difference is not a result of limitations of the Newtonian theory but ensues from the insufficient knowledge of lunar motions on which the estimate is based. Specifically, Brown's formulas for the lunar orbital elements [21] used here do not contain a description of solar-induced tidal phenomena in the Earth–Moon system. These phenomena are taken into account as manifestations of the differences between the anomalistic and tropical months but variations in these differences with a period equal to half the tropical year are not described. The very existence of such variations is well understood and qualitatively characterized by mathematicians [23], but the results of these studies are not supported by observations and have not yielded practical recommendations; in particular, they are not used to interpret tidal phenomena. In what follows, we analyze the gravitational action of the Sun on the relative motion of the Moon and the Earth. The effect of this potential, averaged over the period of revolution of the Moon, accounts for the difference between the tropical (27.322 days) and anomalistic (27.555 days) months. Variations in this potential with a period of 6 months [24] lead to oscillations of the periods and to a frequency modulation of the rotational and oscillatory motions of the Moon. This modulation has a frequency of $2\omega_2$, or a period of half a year.

Let us now consider a heliocentric system of coordinates. Assume that the radius vectors of the centers of the Earth and the Moon are Re and Rm, respectively, the masses of the Sun, Earth, and Moon are S, E, and M, and the universal gravitation constant is G. The Hamiltonian H of the Earth–Moon system can be written in the form [24]

$$H = E\frac{(\mathrm{d}Re/\mathrm{d}t)^2}{2} + M\frac{(\mathrm{d}Rm/\mathrm{d}t)^2}{2} - \frac{GSE}{Re} - \frac{GSM}{Rm} - \frac{GEM}{Re - Rm}\,. \tag{10}$$

The system's center of inertia lies at the point $R = (ERe + MRm)/(E + M)$. Below, we present a theoretical estimate of the frequency modulation of orbital and radial oscillations of the Moon moving in the Earth's gravitational field perturbed by the Sun. The first nonvanishing term in the expansion in powers of the small parameter $D/R \approx 2.5 \times 10^{-3}$ is retained in the analysis (D and R are the distances between the Moon and the Earth and between the Moon and the Sun, respectively). The momenta P_r, P_φ, P_z are considered in cylindrical coordinates with the z axis perpendicular to the Moon's orbital plane with the center coincident with the center of inertia. The components of D are r, z, φ. The motion is described by the Hamiltonian [24]:

$$\frac{1}{2}\mu\left(P_r^2 + \frac{P_\varphi^2}{r^2} + P_z^2\right) - \frac{GME}{r} - \frac{GS\mu r^2}{2R^3}(3\cos\Phi^2 - 1)\,. \tag{11}$$

A correction to the Hamiltonian associated with the solar action is

$$H' = -\frac{GS\mu r^2}{2R^3}(3\cos\Phi^2 - 1)\,. \tag{12}$$

The angle Φ between the directions toward the Sun and the Moon is time-dependent, and $\cos\Phi$ equals

$$\cos MS \cdot \cos\varphi \cdot \cos\omega_2 t + \sin\varphi \cdot \sin\omega_2 t\,,$$

where μ is the reduced mass and $\mu = ME/(E + M)$. The angle $MS = 5°8'43''$ is the mean inclination of the orbit to the ecliptic plane. The quantities

$$\omega_1 = \frac{2\pi}{27.321}\ \mathrm{day}^{-1}\,,\quad \omega_2 = \frac{2\pi}{365.24}\ \mathrm{day}^{-1}$$

are the frequencies of revolution of the Moon and the Sun about the center of inertia, respectively.

The Hamiltonian is a periodic function of time with a period of $2\pi/\omega_2$. The last term is analogous to the solar tidal force in the Moon–Earth system [24]. This is a small adiabatic correction to the interaction potential. It results in the well-known difference between the periods of lunar radial and azimuthal motion [24]. The quantity $\cos MS = 0.9967$ differs very little from unity. These differences will be neglected below. Under this approximation, the Hamiltonian is independent of z, the perturbation does not affect the orbital plane and is a periodic function of time with a period of π/ω_2.

In what follows, the periodic addition is regarded as a small adiabatic perturbation. Unperturbed solutions are well known [25]. The motion occurs in the plane $z = 0$ and is characterized by a constant momentum K with respect to the z axis ($K = \mu r^2\,\mathrm{d}\varphi/\mathrm{d}t$) and the orbit eccentricity $e = 0.055$. The

trajectory is given by the equation

$$\frac{p}{r} = 1 + e\cos\varphi\,. \tag{13}$$

The energy of the Earth – Moon system is

$$W = -\frac{1}{2}\,GME\,\frac{1-e^2}{p}\,.$$

Quantity p is [24]

$$\frac{K^2}{GME} = 384403\ \text{km}\,.$$

The eccentricity e is small. In the first approximation in terms of this small parameter, the orbital motion is represented as uniform revolution in a circle of radius p and radial oscillations with respect to the circle with an amplitude ep and a frequency ω_1 equal to the frequency of revolution. Such a structure of the solution makes up the essence of the small-oscillation method [25]. The model characteristics (the position of the center R_0 and the oscillation frequency ω) can be deduced from the equations of motion using a simple algorithm. The solution is represented in the form $R_0 + r_0(t)$. The distance R_0 relative to which radial oscillations occur is found as the point at which the time derivative of the radial momentum is zero:

$$\frac{\mathrm{d}p_r}{\mathrm{d}t} = -\frac{\partial H'}{\partial r} = 0\,, \quad \text{or} \quad \frac{K^2}{\mu R_0^3} - \frac{GEM}{R_0^2} = 0\,; \tag{14}$$

in the absence of a perturbation, $R_0 = K^2/(GEM) = p$.

Small deviations from the equilibrium r_0 are described by the equation

$$\mu\,\frac{\mathrm{d}^2}{\mathrm{d}t^2}\,r_0 = -\left.\frac{\partial^2 H'}{\partial r^2}\right|_{R_0} r_0 = -\left[\frac{3K^2}{\mu R_0^4} - \frac{2GEM}{R_0^3}\right] r_0 = -\left[\frac{K^2}{\mu R_0^4}\right] r_0\,. \tag{15}$$

It is an equation of oscillations with a frequency $\omega = K/(\mu R_0^2) = \omega_1$. The motion frequency ω can be found from the equation

$$\frac{1}{\mu}\left.\frac{\partial^2 H'}{\partial r^2}\right|_{R_0} = \omega^2\,. \tag{16}$$

Therefore, in the case of small perturbations, the trajectory is represented by a circle relative to which the body undergoes small-amplitude harmonic radial oscillations. The algorithm for estimating the trajectory parameters reduces to the determination of two characteristics — the position of the orbital center [Eqn (4)] and the frequency of radial oscillations, which can be estimated after the calculation of the first term of the expansion of the force at the point of equilibrium into a Taylor series in powers of variable r [Eqn (16)] [25].

We analyze the influence of solar tidal forces on radial oscillations using a small perturbation method. The tidal force has a very weak effect on both rotational and oscillatory motions. The small parameter of the perturbation is the ratio of the characteristic perturbation energy to the relative-motion energy. The perturbation energy is of the order of $GS\mu p^2/R^3$, and the energy of rotational motion is $W = \mu\omega_1^2 p^2$, i.e. the effect of perturbation depends on the small parameter

$$\alpha = \frac{GS}{\omega_1^2 R^3} = \frac{S}{E}\left(\frac{p}{R}\right)^3 = 5\times 10^{-3}\,.$$

This quantity is of the same order of magnitude as $(\omega_1 - \omega_3)/\omega_1 = 8\times 10^{-3}$.

The ratio of the perturbation frequency to the frequency of the proper motion $2\omega_2/\omega_1$ is another small parameter used in the analysis of perturbations. It allows the perturbation to be considered adiabatic [25].

Perturbation of orbital motion. The Hamilton equations for the perturbations of the orbital momentum p_φ are of the form

$$\frac{\mathrm{d}p_\varphi}{\mathrm{d}t} = -\frac{\partial H'}{\partial \varphi}\,. \tag{17}$$

The integration of the perturbation is performed along an unperturbed trajectory for which

$$\mathrm{d}\varphi = \frac{\mathrm{d}t\,\mu r^2}{K}\,. \tag{18}$$

The unperturbed value of the orbital momentum is constant and equals K. Eqns (17), (18) give the following equation for the perturbation p_φ ($P_\varphi = K + p_\varphi$):

$$\frac{\partial p_\varphi}{\partial \varphi} = \frac{GS\,\mu r^2}{2R^3}\,\frac{\mu r^2}{K}\,\frac{\partial}{\partial \varphi'}(3\cos\Phi^2 - 1) = \frac{3\mu\,\omega_1\,p^2\alpha}{(1+e\,\cos\varphi)^4} \times \left\{\cos\varphi\cdot\sin\varphi\,[-\cos^2 MS\cdot\cos^2\omega_2 t + \sin^2\omega_2 t\,] + \cos 2\varphi\cdot\cos\omega_2 t\cdot\sin\omega_2 t\cdot\cos MS\right\}.$$

In estimating p_φ, the eccentricity e is assumed to be small, and an expansion in powers of this quantity is performed. It should be taken into consideration that the period will be calculated based on the estimated action variable [25] I_φ expressed as the integral of momentum over the period:

$$I_\varphi = \frac{1}{2\pi}\int p_\varphi\,\mathrm{d}\varphi\,. \tag{19}$$

The correction to the orbital period T_φ is related to this quantity by the equation

$$T_\varphi = 2\pi\,\frac{\mathrm{d}I_\varphi}{\mathrm{d}W_1}\,. \tag{20}$$

The quantity W_1 is the energy of the Moon's rotational motion.

In calculating the correction to the orbital period, the right-hand side of Eqn (17) is expanded into a Fourier series. Only the leading term of the expansion in eccentricity is retained for each term of the series. This yields

$$\delta M = \frac{9}{16}\,\alpha e^2 K\cos(2\omega_2 t)\,\frac{\omega_1}{\omega_2} - \frac{3}{2}\,\alpha e K\cos(\varphi - 2\omega_2 t)\,\frac{\omega_1}{\omega_1 - 2\omega_2} + \frac{3}{2}\,\alpha K\cos(2\varphi - 2\omega_2 t)\,\frac{\omega_1}{2\omega_1 - 2\omega_2}\,.$$

In estimating slow momentum variations, only the zeroth-order (φ-independent) term should be retained. The terms of the series proportional to $\sin k\varphi$ and $\cos k\varphi$ vanish upon integration with respect to φ in the calculation of the action variable and do not contribute to the change of the period. This term is proportional to e^2 and equals

$$\delta M = \frac{9}{16}\,\alpha e^2\,\frac{\omega_1}{\omega_2}\,K\cos(2\omega_2 t)\,. \tag{21}$$

The correction undergoes a slow time variation with a period of π/ω_2. It describes periodic variations in the orbital momentum and the frequency modulation of the lunar orbital motion. Variations δM in the orbital momentum with a frequency of $2\omega_2$ correspond to the modulation of oscillations with an amplitude equal to

$$\delta T_\varphi = 2\pi\,\frac{9}{16}\,\frac{\alpha e^2}{\omega_2} = 3\times 10^{-3}\ \text{day}$$

in terms of period, or

$$\delta\omega_\varphi = \frac{\omega_1^2}{2\pi}\,\delta T_\varphi = \omega_1^2\,\frac{9}{16}\,\frac{\alpha e^2}{\omega_2} = 2.6\times 10^{-5}\ \text{day}^{-1} \tag{22}$$

in terms of frequency.

This quantity is significantly smaller than $\delta\omega \equiv \omega_1 - \omega_3$. It is virtually unresolvable for the chosen observation interval, which is manifest as the appearance of sharp peaks devoid of a fine structure (Fig. 3c). The additional smallness is related to the parameter $e^2\omega_1/\omega_2 = 3\times 10^{-2}$.

Radial motion. Our analysis of the radial motion proceeds from the representations of small perturbations. The correction δp_0 to the equilibrium position p_0 can be found using Eqn (10) in the form

$$\mu\omega_1^2\,\delta p_0 = \overline{GS\,\frac{\mu r}{R^3}\,(3\cos\Phi^2 - 1)}\,. \tag{23}$$

The right-hand side needs to be averaged over the period of revolution. The leading part of the correction (in parameter e) is time-independent and equals

$$\delta p_0 = \frac{1}{2}\,GS\,\frac{\mu p}{\omega_1^2 R^3} = \frac{1}{2}\,\alpha p\,. \tag{24}$$

Its minor part δp_1 is time-dependent and varies with a frequency of $2\omega_2$. It is proportional to the factor $e^2\,(\omega_1/\omega_2)$.

The correction to the period can be estimated using the equation for small radial oscillations r taking account of the perturbation. It has the form

$$\mu\,\frac{\mathrm{d}^2}{\mathrm{d}t^2}\,r = -\left.\frac{\partial^2 H'}{\partial r^2}\right|_{R_0} r = \left(\frac{12K^2}{\mu R^5} - \frac{6GEM}{R^4}\right)\delta p_r - 3\left[\left(\frac{K^2}{\mu R_0^4} - \frac{2GEM}{R_0^3}\right)r + \frac{GS\mu r}{R^3}\,(3\cos\Phi^2 - 1)\right], \tag{25}$$

or, after the transfer of the perturbation-independent term to the left-hand side,

$$\left(\frac{\mathrm{d}^2}{\mathrm{d}t^2} + \omega_1^2\right) r = \left[\left(\frac{12\,K^2}{\mu^2 R^5} - \frac{6GEM}{\mu R^4}\right)\delta p_r + \frac{GSr}{R^3}\left(\frac{1}{2} + \frac{3}{2}\cos 2\Phi\right)\right]. \tag{26}$$

The time-independent terms in the right-hand side of this equation give a constant correction to the frequency of radial oscillations which, in accordance with Eqn (15), equals

$$2\omega_1\,\delta\omega_r = \left[-\left(\frac{12K^2}{\mu^2 R^5} - \frac{6GEM}{\mu R^4}\right)\delta p - \frac{GS\,r}{R^3}\,\frac{1}{2}\right]\frac{1}{2\omega_1}\,,$$

or

$$\delta\omega_r = -1.75\,\alpha\omega_1\,. \tag{27}$$

This known correction determines the differences between the periods of radial and orbital motions of the Moon and equals the known value $\omega_3 - \omega_1$.

In order to find the time-dependent correction to the frequency, only the terms changing with frequencies close to ω_1 need to be distinguished.

In the term $(GSr/R^3)(3/2)\cos\left[2(\varphi - \omega_2 t)\right]$,

$$\begin{aligned} &r\cos\left[2(\varphi - \omega_2 t)\right] \\ &\quad = ep\cos\varphi\left[\cos 2\varphi\cdot\cos(2\omega_2 t) + \sin 2\varphi\cdot\sin(2\omega_2 t)\right] \\ &\quad = \frac{1}{2}\,ep\left[\cos\varphi\cdot\cos(2\omega_2 t) + \cos 3\varphi\cdot\cos(2\omega_2 t)\right. \\ &\quad\quad \left. + \sin\varphi\cdot\sin(2\omega_2 t) + \sin 3\varphi\cdot\sin(2\omega_2 t)\right]. \end{aligned}$$

In this term, the only component surviving after averaging over the period is $(1/2)\,ep\cos\varphi$. The remaining components vanish upon averaging and do not contribute to frequency variations.

The expression

$$2\omega_1\,\delta\omega_2 = \frac{GS}{R^3}\,\frac{3}{2}\,\frac{1}{2}\,\cos(2\omega_2 t)\,,$$

holds for the variable frequency component, and the expression

$$\delta\omega_2 = \frac{3}{8}\,\alpha\omega_1\,. \tag{28}$$

does so for the amplitude of frequency modulation $\delta\omega_2$.

In summary, the action of the Sun on the Moon – Earth system is characterized by the small parameter $\alpha = (S/E)(p/R^3) \approx 5\times 10^{-3}$ and reduces to a small change in the equilibrium distance between the Moon and the Earth $\delta p_0 = (3/2)\,\alpha p$, to the appearance of the difference $\delta\omega = 1.75\alpha\omega_1 = 0.002\ \text{day}^{-1}$ between the mean frequencies of orbital and radial oscillations, and to the frequency modulation of orbital ($\delta\omega_\varphi$) and radial ($\delta\omega_{r2}$) lunar motions that occurs with a frequency of $2\omega_2$ and amplitudes of

$$\delta\omega_{1\varphi} = \omega_1^2\,\frac{9}{16}\,\frac{\alpha e^2}{\omega_2} = 2.6\times 10^{-5}\ \text{day}^{-1},$$
$$\delta\omega_2 = \frac{3}{8}\,\alpha\omega_1 = 4.5\times 10^{-4}\ \text{day}^{-1}.$$

The amplitude of the frequency modulation of radial oscillations is much larger than that of the modulation of rotation. This can be accounted for by the fact that these motions separate in the approximation of small perturbations, and the total energy is represented as the sum of these quantities. The energy of rotation W_1 is much larger than the oscillation energy W_1. The latter is proportional to the square of the eccentricity and equals $W_2 = e^2p^2\omega_1^2/2 = e^2W_1$ for an unperturbed motion. Modulation of radial oscillations can be seen in the spectra constructed from the data for 20 years. For this reason, the proper structure of the line produced by the frequency modulation of radial oscillations of the Moon is

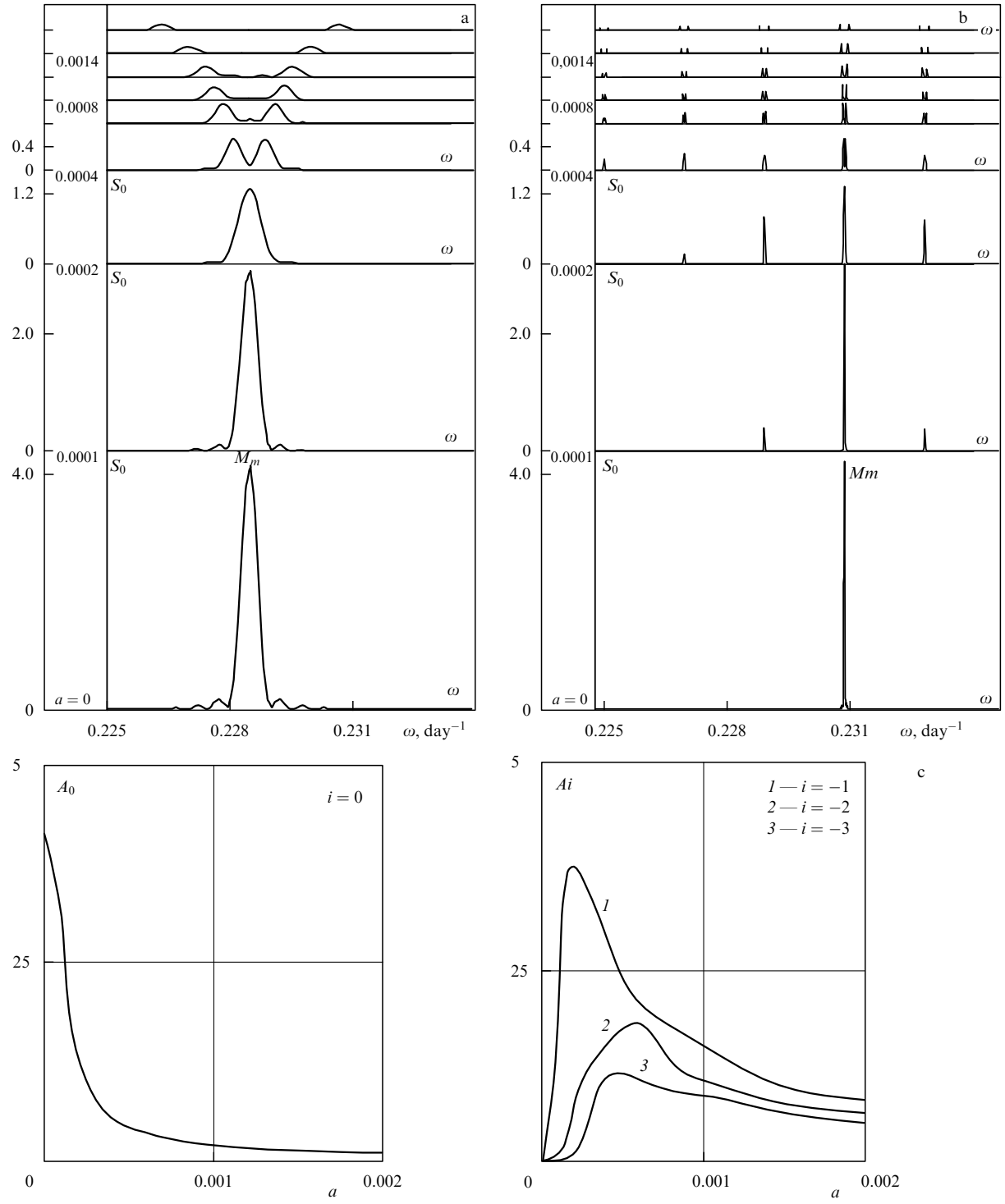

Figure 5. (a) Spectra S_0 of frequency modulated oscillations at different values of the modulation amplitude a (day^{-1}). Amplitude values are indicated near the corresponding lines. The fundamental frequency is $Mm = 0.23$ day^{-1}. The main maximum is depicted in detail. The modulation frequency is $2S = 0.0344$ day^{-1}. The ordinate is given in arbitrary units common for all the curves. (b) Spectra S_0 of frequency modulated oscillations at different values of the modulation amplitude a. Amplitude values are indicated near the corresponding lines. The figure illustrates the amplitudes and positions of the lines at combination frequencies $Mm - i2S$ ($i = \pm 1, 2, 4$). (c) Plots of the spectral-maximum amplitudes Ai at combination frequencies versus modulation amplitude a. The dependence is shown for the maxima with $i = 0, 1, 2, 3$.

most conveniently observed using the line Mm (frequency ω_3) in the spectrum of sea-level fluctuations. It is assumed in the theory of tides that this line is produced by lunar radial oscillations. Certain features of the spectrum of the frequency-modulated oscillation are illustrated below for a main fluctuation period of 27.555 days and its variations with a frequency-oscillation amplitude of $(1-20)\times10^{-4}$ day^{-1}. The spectrum is calculated based on the data obtained at a 2-day interval during an observation period of 40 years. The results are represented at a frequency interval of 10^{-4} day^{-1}. The same software is used as for the calculation of real oscillation spectra, that is the spectrum of

quantity

$$Y(t) = \cos\left[\left(\omega_3 + a\cos(2\omega_2 t)\right)t\right]$$

is calculated for the values

$a = 0$, 0.0001, 0.0002, 0.0004, 0.0006, 0.0008; 0.001, 0.0014, 0.002 day^{-1}.

The results are shown in Fig. 5. Figure 5a represents the results of calculations at different values of parameter a in the vicinity of the main oscillation frequency, Fig. 5b the results of calculations in a broader region containing several combination maxima, and Fig. 5c the dependence of the amplitudes of the main and the first combination maxima on the modulation amplitude a.

Evidently, the peak broadens with increasing a while its amplitude decreases. At a theoretical value of $a = 0.0004$, it splits into three: the central peak at frequency ω_3 and two side peaks at frequencies $\omega_3 \pm a$. At large a, the amplitude of the peaks decreases with increasing a as $1/a^{1/2}$. The splitting of the maximum caused by the modulation of the radial oscillation frequency has a marked effect on the estimates of the amplitude of these oscillations. The dependence is shown in Fig. 5c. It can be seen that, for the theoretical value of the period-modulation amplitude, this effect is responsible for a more than 10-fold decrease in the observed line amplitude.

The results thus obtained are in excellent agreement with the expected ones. Variations of the signal frequency within $2a$ naturally lead to a broadening of the line by this quantity and a decrease in its amplitude. This results in the line acquiring two maxima located at the boundaries of the band.

It can be concluded that frequency modulation of variations in the distance between the Moon and the Earth accounts for a broadening of the spectral maximum Mm due to its splitting into three peaks — the central one and two others, shifted by the value of the modulation frequency. Simultaneously, the amplitude of the maximum decreases, and combination maxima appear at frequencies $\omega_3 \pm l2\omega_2$, where l is an integer. Each combination maximum is split into two spikes located symmetrically with respect to the unperturbed position of line c at a distance of $\delta\omega$ from it.

Similar effects, i.e. the broadening of the maximum, the appearance of a few closely located peaks instead of a single one, and a large number of additional peaks at combinations of the fundamental frequency with frequency $2\omega_2$, are also observable at any combinations of tidal-potential frequencies, including the radial-oscillation frequency. Specifically, this is true of lines (1, 0, −1), (1, 1, −1), (1, −1, 1), which split and therefore give rise to a comb-like line pattern clearly seen in the spectrum (Fig. 5b).

4.3 Spectrum of modulations of solar irradiance during eclipses

The influence of the Moon on the Earth's atmosphere manifests itself through two well-studied mechanisms. One is the partial reflection of solar radiation by the Moon, the other is the solar eclipse. We considered spectra of solar-irradiance variations caused by these mechanisms.

To estimate the moonlight illuminance of the Earth's surface, we assumed that it depends on the angle Φ between the directions from the Earth to the Moon and the Sun. The same system of coordinates as in the preceding Section (Fig. 4a) was used for computations. In this system, the z axis is normal to the ecliptic plane (the plane of the Earth's revolution around the Sun). Axis y coincides with the line of intersection of the planes of the lunar orbit and the ecliptic. The origin coincides with the center of the Earth. This system of coordinates rotates in space about the z axis with the frequency SAR.

The cosine of angle Φ determining the lunar phase is

$$\cos\Phi = \cos MS\cdot\cos(M+SAR)\,t\cdot\cos(S+SAR)\,t + \sin(M+SAR)\,t\cdot\sin(S+SAR)\,t\,. \qquad (29)$$

The spectrum was calculated taking into consideration the observed phase dependence of the lunar brightness [20]. Its deviation from the Lambert law is large enough to affect the intensity distribution among individual lines. This dependence was used to find the time variations in the full illuminance of the Earth by the solar radiation scattered from the lunar surface. These variations provided a basis for the construction of perturbation spectra. Of the three periods, M, S, and SAR, only lines corresponding to the harmonics of the period $M - S$ actually occur in the spectrum. The observable peaks corresponding to other combinations of periods have very small amplitudes (more than four orders of magnitude smaller than the amplitudes of the maxima of main-period harmonics). This finding can be accounted for by the smallness of the difference of $\cos MS$ from unity. When $\cos MS = 1$, the expression (29) for $\cos\Phi$ contains only $\cos(M-S)\,t$, being independent of other frequencies. The fundamental harmonic corresponds to frequency $M - S$; the second one in terms of intensity, to $2M - 2S$ (it is approximately 7 times lower); and the third, to $3M - 3S$ (a few per cent of the intensity of the main one).

One more cause underlying the modulation of solar-radiation effects is worth mentioning [26, 27]. This is the Earth's rotation about its axis accounting for the clear division of the globe into two hemispheres. The energy exchange between the hemispheres is much less effective than within a given hemisphere. This effect is the main source of seasonal variations in temperature and pressure. It can be roughly estimated from the modulation of the total energy flux incident on the northern hemisphere (but not on the entire globe). Such a modulation is due to the tilt of the Earth's axis relative to the normal to the ecliptic plane. The angle of inclination is $E = 23°26'45''$. In this case, the amount of energy that reaches the northern hemisphere is

$$\frac{1}{2}\left(1 + \sin E\cdot\cos(St + \Phi_1)\right),$$

where Φ_1 is the phase of the Earth's revolution around the Sun at the new Moon — the time used as a reference point. This variation produces a spectral line with frequency S.

It should be noted that such a modulation is absent in the case of solar radiation reflected by the lunar surface and reaching the Earth. However, even in this case, a separate analysis of the flux coming to the northern hemisphere should take into account the tilt of the Earth's axis relative to the lunar orbit (angle EM). The additional modulation of the radiation reflected by the Moon is

$$\frac{1}{2}\left(1 + \sin EM\cdot\cos M(t + t_1)\right).$$

The quantity EM changes with time as a result of the regression of the lunar orbital nodes in a range from $18°18'$ to $28°35'$. Changes in the sine of this angle with time can be

described by the equation

$$\sin EM = \sin E \cdot \cos MS + \cos E \cdot \sin MS \cdot \cos(SAR\, t)\,.$$

For this reason, less intense but clearly observable lines are added to the pronounced lines at the harmonics of the frequency $M - S$; the additional lines have the frequencies

$$S \pm SAR\,,\quad M - 2S \pm SAR\,,\quad M \pm SAR\,,$$
$$2M - 3S \pm SAR\,,\quad 2M - S \pm SAR\,,\quad \text{etc.}$$

The most intense of them (lines $S \pm SAR$ and $2M - S \pm SAR$)) arise from the additional modulation of oscillations corresponding to the main spectral line $M - S$.

Thus, the solar radiation reflected by the Moon is responsible for the periodic modulation of the Earth's temperature and produces specific lines at synodic-period harmonics. The Earth's rotation about its axis gives rise to somewhat weaker lines at combinations of these harmonics with frequencies $M + SAR$ and $M - SAR$. However, this effect is much (about 1000 times) smaller than that of eclipses. The modulation of radiation and its spectrum are shown in Fig. 6.

The spectra of solar eclipses are considered below. It is assumed that the main effect of an eclipse is the obscuration of the solar energy flux that illuminates the Earth's surface. On a sphere of radius D (D is the distance between the Moon and the Earth), this flux is formed over a circular area O_1 of radius $R_1 = a + (r_S - a)\, D/R_S$ with its center at the intersection of the sphere's surface by the direction from the Earth to the Sun. Here $a = 6370$ km is the radius of the Earth and $r_S = 695\,600$ km is the Sun's radius. The angular size of this circle is

$$\theta_0 = \frac{R_E + (R_S - R_E)\, D/R_S}{D} = 0.0211\,.$$

When an eclipse occurs, part of this circle is darkened by the Moon. This part is as large as the area of intersection of the circle O_1 with the circle O_2 at the surface of the same sphere with the center at the point of its intersection by the direction towards the Moon and with a radius of r_m (r_m is the radius of the Moon, 1730 km). The angular size of this circle is

$$\theta_m = \frac{r_m}{D} = \frac{1730}{384000} = 0.0045\,.$$

The geometry of occultation is illustrated in Fig. 4b. It results in reducing the Earth's illuminance in proportion to the ratio of the area of intersection of circles O_1 and O_2 to the area of circle O_1. This ratio depends on the angle Φ between the directions to the Sun and the Moon, the cosine of which is given by formula (29). Figure 4c shows the phase dependence of the shadowing used for spectrum computation. The shadowing effect is absent when $\Phi > \theta_0 + \theta_m$ and equals $Sh = (\theta_m/\theta_0)^2 = 0.0455$ when $\Phi < \theta_o + \theta_m$. In an intermedi-

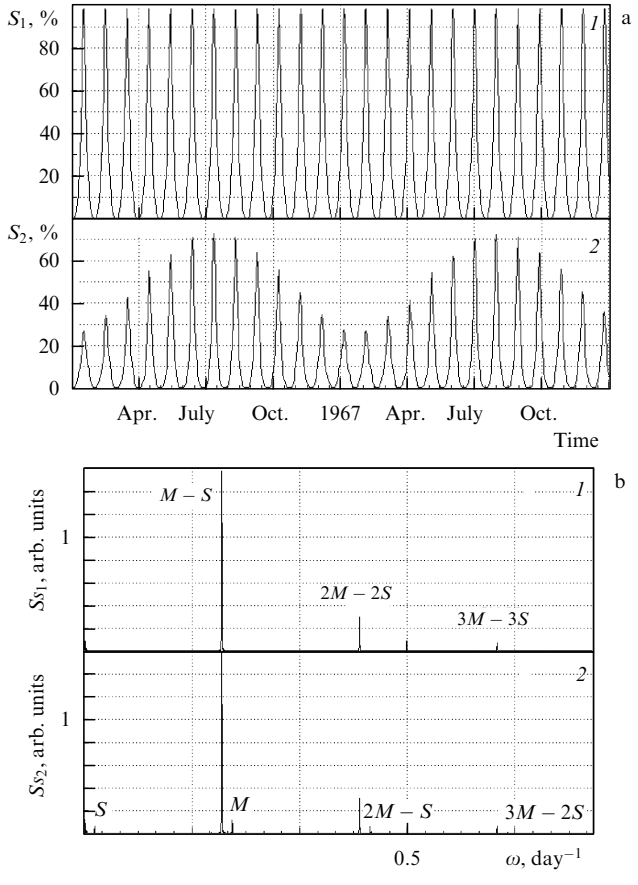

Figure 6. (a) Modulation of the intensity of solar radiation scattered from the Moon to the Earth's surface, S_1, and to the northern hemisphere, S_2, in percent of the total. (b) Spectrum of solar radiation scattered by the Moon to the Earth's surface, Ss_1, and to the northern hemisphere, Ss_2, in arbitrary units.

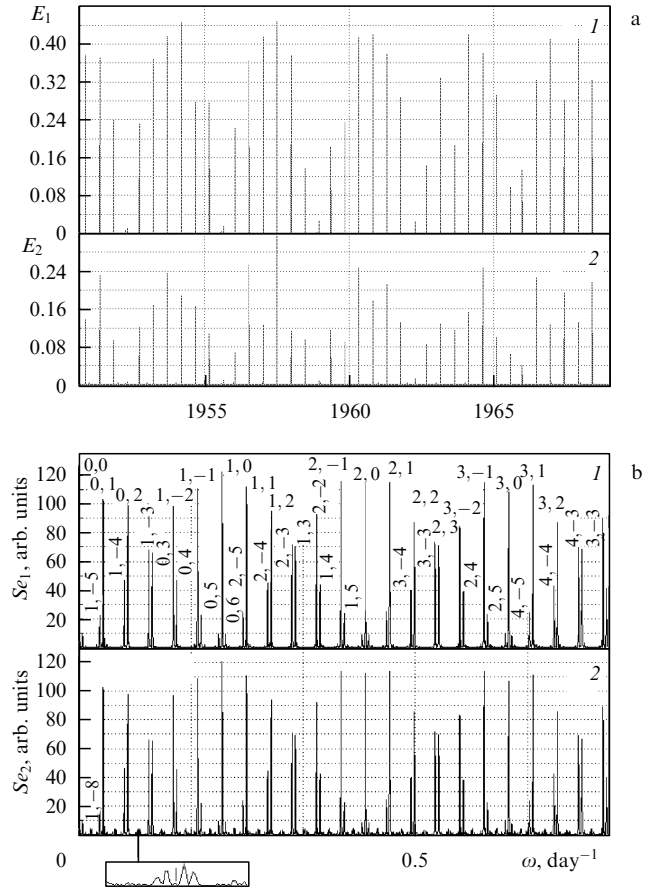

Figure 7. (a) Time dependence of the occultation of the Sun by the Moon for the whole Earth, E_1, and for the northern hemisphere, E_2, (fraction of the total flux). (b) Spectra of the time dependence of the occultation of the Sun by the Moon for the whole Earth, Se_1, and for the northern hemisphere, Se_2, in arbitrary units.

ate case, this effect can be evaluated using the system of equations

$$\theta_0 \sin\varphi_1 = \theta_m \sin\varphi_2\,,$$
$$\theta_m(1-\cos\varphi_1) + \theta_0(1-\cos\varphi_2) = \Phi\,,$$
$$Sh = \frac{1}{\pi}\left(\theta_0(\varphi_1 - \sin\varphi_1) + \theta_m(\varphi_2 - \sin\varphi_2)\right). \qquad (30)$$

The time dependence of the shadowing effect is shown in Fig. 7a (graph *1*), and the spectrum of this quantity in Fig. 7b (graph *1*).

The spectrum is a series of bands with a central frequency equal to $M - S$; also present is a band corresponding to zero frequency. An individual band contains a set of equidistant lines located at an interval of $2S + 2SAR$. Each line is characterized by two integers, the band number $i = 0$, 1 and the line number in the band k, which may be either positive or negative. Therefore, the frequencies of the main lines are given by the formula

$$\omega_{i,k} = (M - S)\,i + (2S + 2SAR)\,k\,. \qquad (31)$$

In Fig. 7b (graph *1*), each line is labeled by the numbers, i and k. At first sight, such a spectral pattern looks surprising because the argument of the function $\sin\Phi$ virtually reduces to a periodic function with a period of $M - S$. Deviations from this periodic function have an order of magnitude of $(1 - \cos SM) \sim 0.004$. Therefore, the spectrum should seemingly be composed of lines at harmonics of the frequency $M - S$, as the spectrum of the Earth's illuminance by the light scattered from the Moon. Marked deviations from this situation occur because the function undergoes substantial changes within a very small interval $\sim \theta_0$. In order to estimate the number of significant harmonics for the period $2S + 2SAR$, SM should be compared with θ_0, which is about 3 times smaller. Therefore, approximately three harmonics for the additional period $2S + 2SAR$ are of the same order of magnitude. Due to the properties of the dependence of Sh on θ, the intensities of other lines in the band decrease relatively slowly, which accounts for the presence of more than 10 lines in a single band, and bands markedly overlap. In the region of overlapping, lines of similar intensity form doublets. One such line belongs to the left band, and the other to the right one. The gap between the two lines is $\sigma = 13S + 12SAR - M = 0.0051$ day^{-1}. In the time dependence, spectral doublets are manifest as beats of the intensity of eclipse action with a period of $2\pi/\sigma = 1228.87$ days.

The eclipse spectrum looks slightly modified if the modulation of the light flux is considered for the northern hemisphere alone. In this case, the intensity of shadowing calculated with formula (2) should be multiplied by $(1/2)\big(1 + \sin E \cdot \cos(St + \Phi_1)\big)$. As a result, each line acquires two additional lines shifted by the frequency $\pm S$ and

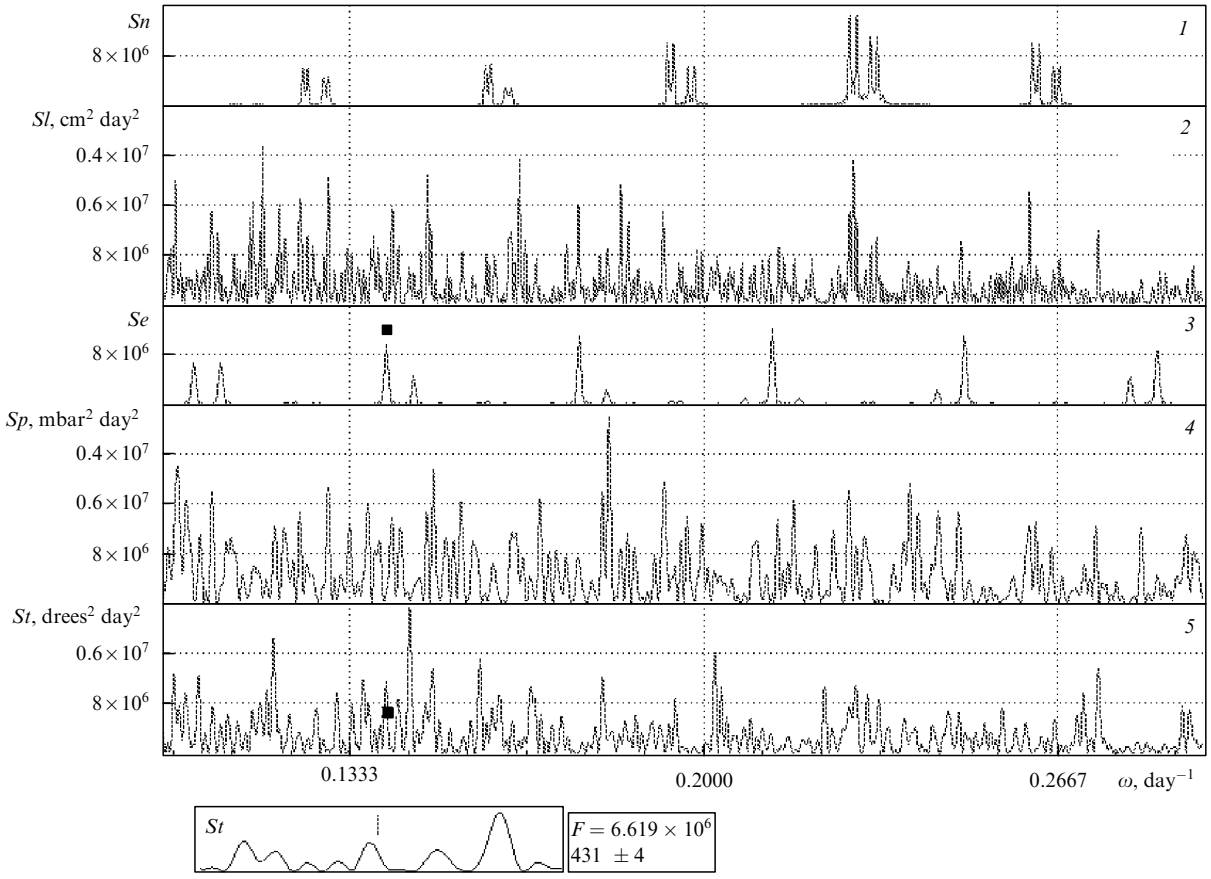

Figure 8. Illustration of the procedure of comparing the spectral maxima of the air temperature, atmospheric pressure, and sea level with the theoretical spectra. The theoretical line in the eclipse spectrum is indicated by a square. The inset at the bottom shows amplitude variations in the air-temperature spectrum in the vicinity of the theoretical peak. Graph *1*, spectrum *Sn* of the lunar tidal potential taking into account the frequency modulation of radial oscillations; *2* , spectrum *Sl* of sea-level fluctuations; *3*, spectrum *Se* of eclipses; *4* and *5*, spectra *Sp* and *St* of the atmospheric pressure and temperature, respectively.

having 4% of the intensity of the perturbed line. The dependence of flux modulation for the northern hemisphere is shown in Fig. 7a (graph *2*), and the spectrum in Fig. 7b (graph *2*). The additional lines are separate narrow bands composed of four or six lines each.

The most interesting feature is the periodic modulation of the energy flux with a period of 1229 days (3.4 years). Such a modulation manifests itself in the spectra as a line splitting into doublets. The spectrum under consideration contains many lines and provides sufficient material for comparisons with the observed spectra.

4.4 Comparison of the observed and eclipse spectral lines

The sources of periodic meteorological perturbations in a range from 10 to 60 days considered above are not the prevalent ones nor do they produce the most pronounced variations. Nevertheless, they are fairly intense and can be reliably identified by the spectral analysis of observation series for a period of 20 years or more. The appearance of these lines provides convincing evidence for the reality of the line spectral structure and allows using all the observed lines for long-term weather forecasting. Deviations from the theory make it possible to improve our notion of lunar motion, which is important for investigations into the evolution of the Solar System [28, 38].

In what follows, the theoretical lines of perturbation spectra produced by solar eclipses and specific features of the lunar-tidal-potential spectrum related to the frequency modulation of distance variations are compared with the spectra of sea-level fluctuations and variations in atmospheric parameters. The procedure of comparison is illustrated by Fig. 8. Graphs *1* and *3* show, at a convenient scale, theoretical spectra of lunar-tidal-potential perturbations associated with the specific features of variations in the distance between the Moon and the Earth and during eclipses. Graphs *2*, *4*, and *5* show the spectra of sea-level, atmospheric-pressure, and air-temperature variations, respectively. After a theoretical spectral line (indicated by a small square in the figure) is chosen, the spectrum of the parameter of interest is analyzed in the vicinity of a selected point. Such a vicinity is shown on a larger scale in the inset at the bottom of the figure. The frequency at the selected point corresponds to the vertical line in the upper part of the inset.

The peak closest to the selected point or the highest of the nearest maxima (if the distances to the maxima on the left and on the right are equal) is chosen for the purpose of comparison. The peak frequencies and amplitudes are taken from the graphs; they are listed in Tables 5 and 6. Table 5 analyzes spectral lines of sea-level fluctuations at point Kholmsk for a period of 40 years. Table 6 analyzes spectral lines of air-temperature and atmospheric-pressure variations at point Terneĭ for 18 years with a resolution of 10^{-4} s^{-1}. The results of comparison are represented separately for the lines of tides and eclipses.

The results of comparison of tidal lines and the sea-level fluctuation spectrum are presented in Table 5. Each line is described by the numbers i, j, k, l and the sign + or −. The characteristics of lines i, j, k, l are related to frequency ω through the expression $\omega = i\,\omega_1 + j\,\omega_3 + k\,\omega_4 + l\,\omega_2 \pm \beta$. Only the main lines with $i = 0$ and $i = 1$ were analyzed. The sign in the line index corresponds to the sign in the formula; β is the modulation amplitude of the radial-oscillation frequency. For each line, the period and amplitude of the maximum are calculated in a discrete representation of the dependence at a frequency step of 0.98×10^{-4} day^{-1}.

In Table 6, only the most intense lines of the eclipse spectrum are analyzed, i.e. the lines that make up doublets at frequencies $i(M - S) + k(2S + 2SAR)$. The parameters of

Table 5. Spectral lines of tidal potential and sea level fluctuations*.

No.	Multipliers in frequency combinations: i at ω_1, j at ω_3, k at ω_4, and l at ω_2. In column l, the sign behind a number corresponds to the sign of the frequency deviation β				Theoretical estimates of line characteristics: 1, period (days); 2, spectral amplitude (cm^2 day^2)		Estimates of observed line characteristics: 3, period (days); 4, spectral amplitude (cm^2 day^2)	
	i	j	k	l	1	2	3	4
1	0	1	0	−3−	50.51	5.9	50.71	16.0
2	0	1	0	−3+	50.15	5.8	50.15	11.0
3	0	1	0	−2−	39.58	6.2	39.55	7.8
4	0	1	0	−2+	39.33	6.4	39.38	6.0
5	0	1	0	−1−	32.55	10.0	32.65	12.0
6	0	1	0	−1+	32.36	9.7	32.36	2.3
7	0	1	0	0−	27.63	14.0	27.63	14.8
8	0	1	0	0	27.55	3.8	27.55	22.0
9	0	1	0	0+	27.46	14.0	27.46	12.0
10	0	1	0	1−	23.99	9.9	23.99	4.1
11	0	1	0	1+	23.88	9.8	23.90	4.9
12	1	−1	0	−3−	48.96	4.25	48.91	7.5
13	1	−1	0	−3+	48.63	4.25	48.63	20.0
14	1	−1	0	−2−	38.62	2.35	38.49	10.0
15	1	−1	0	−2+	38.39	2.6	38.39	11.0
16	1	−1	0	−1−	31.90	6.0	31.95	4.0
17	1	−1	0	−1+	31.71	6.0	31.64	8.6
18	1	−1	0	0−	27.16	10.5	27.14	8.5
19	1	−1	0	0+	27.01	11.0	27.02	11.0
20	1	−1	0	1−	23.64	6.0	23.64	5.3
21	1	−1	0	1+	23.53	6.0	23.53	7.3

* $\omega_1 = 2\pi/27.332 = 0.2299$ day^{-1}, $\omega_2 = 2\pi/365.25 = 0.0172$ day^{-1}, $\omega_3 = 2\pi/27.555 = 0.2280$ day^{-1}, $\omega_4 = 2\pi/6585.32 = 0.00095$ day^{-1}, $\beta = 0.00045$ day^{-1}. Estimated values of spectral maximum amplitudes are multiplied by 10^6.

Table 6. Comparison of eclipse spectral lines with the spectra of sea-level, atmospheric-pressure and temperature variations.

No.	Eclipse spectrum			Sea-level fluctuations		Pressure variations		Temperature variations	
		period	amplitude	period	amplitude	period	amplitude	period	amplitude
1	−1, 6	1230	0.9	1254.9	2×10^7	1333	8.3×10^7	1255	5.1×10^7
2	1, −5	202.5	2.1	203.17	2.8×10^7	201.2	16×10^7	205	15×10^7
3	0, 1	173.9	10.0	172.04	1.95×10^7	173.9	52×10^7	171	34×10^7
4	1, −4	93.02	4.5	92.48	7×10^6	93.43	12×10^7	92.75	11×10^7
5	0, 2	86.48	9.7	85.56	13×10^6	85.2	15×10^7	85.21	22×10^7
6	1, −3	60.60	6.6	60.26	6×10^6	59.8	20×10^7	59.98	12×10^7
7	0, 3	57.76	6.5	57.70	4.9×10^6	58.44	28×10^7	57.7	4.6×10^7
8	1, −2	44.81	9.6	44.78	7.5×10^6	44.47	26×10^7	44.81	11×10^7
9	0, 4	43.24	4.5	43.24	4.7×10^6	42.95	8.5×10^7	43.06	3.4×10^7
10	1, −1	35.63	10.0	35.65	16×10^6	35.63	14×10^7	35.45	1.6×10^7
11	0, 5	34.63	2.2	34.59	20×10^6	34.48	59×10^7	34.68	11×10^7
12	2, −6	30.2	1.0	30.24	1.05×10^6	30.21	2.8×10^7	30.24	4.2×10^7
13	1, 0	29.52	12	29.37	9.1×10^6	29.35	27×10^7	29.52	3×10^7
14	0, 6	28.88	0.6	28.78	1.2×10^6	28.78	9.4×10^7	28.86	0.6×10^7
15	2, −5	25.76	2.3	25.69	1.9×10^6	25.71	29×10^7	25.81	4.5×10^7
16	1, 1	25.23	11.0	25.30	8.5×10^6	25.29	28×10^7	25.17	2.6×10^7
17	2, −4	22.40	4.0	22.37	1.9×10^6	22.32	1.4×10^7	22.43	0.1×10^7
18	1, 2	22.00	9.3	21.98	5×10^6	21.97	9×10^7	21.97	0.26×10^7
19	2, −3	19.85	7.0	19.89	4.9×10^6	19.85	19×10^7	19.82	2.2×10^7
20	1, 3	19.53	6.9	19.54	1.9×10^6	19.53	14×10^7	19.52	7.4×10^7
21	2, −2	17.81	7.3	17.80	2.7×10^6	17.82	12×10^7	17.81	4.6×10^7
22	1, 4	17.54	4.2	17.54	0.3×10^6	17.55	10×10^7	17.53	3.4×10^7
23	2, −1	16.14	11.0	16.09	8.1×10^6	16.14	13×10^7	16.18	5.5×10^7
24	1, 5	15.93	2.2	15.91	1.2×10^6	15.90	18×10^7	1.589	5.3×10^7
25	3, −6	14.93	0.85	14.90	4×10^6	14.92	3.4×10^7	14.92	1.6×10^7
26	2, 0	14.76	11.2	14.73	4.9×10^6	14.72	24×10^7	14.73	16×10^7
27	1, 6	14.58	0.83	14.57	4.0×10^6	14.57	7×10^7	14.57	2.6×10^7
28	3, −5	13.75	2.4	13.74	6.9×10^6	13.76	10×10^7	13.76	4.4×10^7
29	2, 1	13.61	11.0	13.56	6.2×10^6	13.56	16×10^7	13.58	8.9×10^7
30	3, −4	12.74	4.0	12.75	4.5×10^6	12.71	8.5×10^7	12.73	1.9×10^7
31	2, 2	12.61	7.9	12.62	2.3×10^6	12.62	9.2×10^7	12.61	4.8×10^7
32	3, −3	11.86	7.1	11.86	4.2×10^6	11.86	10×10^7	11.87	4.2×10^7
33	2, 3	11.75	6.9	11.74	3.2×10^6	11.72	9.2×10^7	11.75	2.8×10^7
34	3, −2	11.11	8.32	11.105	3.2×10^6	11.11	3.6×10^7	11.12	6.7×10^7
35	2, 4	11.01	3.8	11.00	1.7×10^6	11.00	6.3×10^7	11.01	2.8×10^7

lines i and k are given in the second column. The third and the fourth column contain the theoretical period in days and intensity in arbitrary units for the given line.

The spectra were computed in units used for the purpose at the Far East Hydrometeorological Institute. They are 0.1 cm for sea level, 0.1° for temperature, and 0.1 mbar for pressure. The unit of time is 1 day.

The following features are worth noting:

1. The discrepancy between the estimates for different periods does not exceed a few units of the last digit. It is somewhat smaller for sea-level fluctuations than for variations in the atmospheric pressure and temperature.

2. For periods shorter than 40 days, the locations of maxima in the spectra of sea-level, atmospheric-pressure, and temperature variations virtually coincide with the theoretical ones. For smaller frequencies, the deviations are attributable to the errors arising from calculations with an insufficient frequency resolution. However, they may also be due to incorrect interpretation of low-frequency maxima, the amplitudes of which are several times higher than the theoretical ones.

3. There are marked differences between the estimated amplitudes of individual lines. These differences are especially pronounced for temperature and pressure spectra and smaller for the spectra of sea-level fluctuations (Fig. 8, graph for *Sl*). I believe that it is due to the dependence of eclipse manifestations on the geographic position of the observation point. This dependence is more important for atmospheric phenomena than for sea-level fluctuations.

4. As a rule, the intensity of spectral lines of atmospheric-parameter variations is several times larger than the theoretical value.

This fact is of little surprise. A comparison of the intensities of diurnal and seasonal variations of atmospheric parameters reveals an approximately thrice lower efficiency of changes in the solar thermal flux, in terms of the formation of seasonal variations. This is a general property of atmospheric processes, which tend to level spatial variations caused by extraatmospheric factors. Being most essential for seasonal variations, such a leveling effect is also manifest in the case of daily variations.

Thus, modulation of solar illuminance during eclipses produces strictly periodic lines in the spectra of atmospheric-pressure and temperature variations at frequencies $\omega_{i,k} = (M - S)\, i + (2S + SAR)\, k$. Modulation of lunar radial oscillations with a frequency of $2S$ and an amplitude of $\beta = 4 \times 10^{-4}$ day^{-1} leads to the splitting of all lunar-tide lines into doublets with a 2β-wide gap between them and to the appearance of additional doublets at combinations of the fundamental and $2S$ frequencies. These lines are readily observable in the spectra of sea-level, atmospheric-pressure, and temperature variations, being evidently a physical fact rather than 'spurious maxima attributable to specific properties of the spectra'. However, they are not the main lines, and

there are many other lines of unknown origin which may be no less important, as it appears from the materials of observations taken alone. These lines can also be used to compose long-term weather forecasts for a period determined only by the line width.

Moreover, analyses of such spectra of climatological parameters provide valuable information for astronomical investigations, e.g. for the study of the evolution of the Earth – Moon system [28]. In the case considered above, this is information about the frequency modulation of variations in the distance between the Earth and the Moon. It may be used to obtain additional results. Specifically, an estimate of the line amplitude at a frequency of $2\omega_1 + 2\omega_2$ gives an estimate for the amplitude of frequency modulation of the lunar revolution frequency. This line can readily be resolved from an adjacent line, $2\omega_1 + 2\omega_2 + 4\omega_4$, attributable to the effect of eclipses. It appears as a combination line related to the main tidal component at a frequency of $2\omega_1$. There is no splitting of the central line at the given duration of the observation period, and the combination line is weak. The ratio ζ of spectral amplitudes at the first combination and at the fundamental frequency can be estimated using the expression $\zeta \cong (\delta\omega_\varphi T)^2/16$. This line is pronounced in the spectrum of sea-level fluctuations, and the ratio ζ is 3.2×10^{-3}. For the amplitude $\delta\omega_\varphi$, this ratio is 1.56×10^{-5} day^{-1}, in agreement with the theoretical value 2.6×10^{-5} day^{-1}. Since a small maximum located not very far from higher peaks is considered, such a coincidence can be regarded as satisfactory.

5. The role of coherent pressure variations in weather formation

5.1 Prediction of variation trends

The principal merit of purely periodic variations is the possibility of accurately predicting them for a long period. Such variations are distinguished during observations as narrow spectral lines whose width depends on the time interval for which the spectrum is calculated. It follows from the above spectra of atmospheric-pressure and air-temperature variations that such lines contain up to 50% of the energy of the signal with seasonal variations subtracted. Variations $y(t)$ can be predicted by summation of harmonic components:

$$y(t) = \sum A_i \cos(\omega_i t - \varphi_i)\,. \tag{32}$$

The frequencies ω_i of individual components are determined from the positions of narrow spectral maxima, amplitudes A_i from spectral peak values, and phases from the ratio of the sine and cosine components of the spectrum deduced by an additional analysis. This prognostic method was first proposed by Laplace [7] and is still in use while predicting tidal sea-level fluctuations. This approach makes it unnecessary to understand the nature of variations, although such understanding increases the reliability of prediction. The prognostic procedure has been realized in the form of a code written in TURBO PASCAL. The code permits the use of series of initial variations from 7800 points and yields prognostic data for 2000 points over a certain period ahead. The spectra are obtained by representing the Fourier transform as a polynomial of a complex variable

$$z = \cos(\omega\delta T) + i\,\sin(\omega\delta T)\,,$$

where δT is the interval of signal discretization. Polynomials of high degree are calculated by the well-known Horner procedure [29], and the calculation of one spectrum takes less than 2 min (Pentium, 133 MHz). The spectrum calculated from the initial data is displayed on the monitor screen, and the operator selects interactively the maxima i to be used in composing a prognosis based on formula (32). The quality of such a prognosis is illustrated in Fig. 9, where graphs *4* and *6* are used to compare the observed and theoretical variations of atmospheric pressure at point Terneĭ.

The above analysis suggests the possibility of forecasting long-term variations of atmospheric pressure (with periods over 10 days) for a few years in advance. However, these variations taken alone are insufficient to fully characterize weather conditions. In technological and social contexts, it is most important to predict the wind speed and precipitation. The possibility of reliable prediction of the latter will be considered in this section.

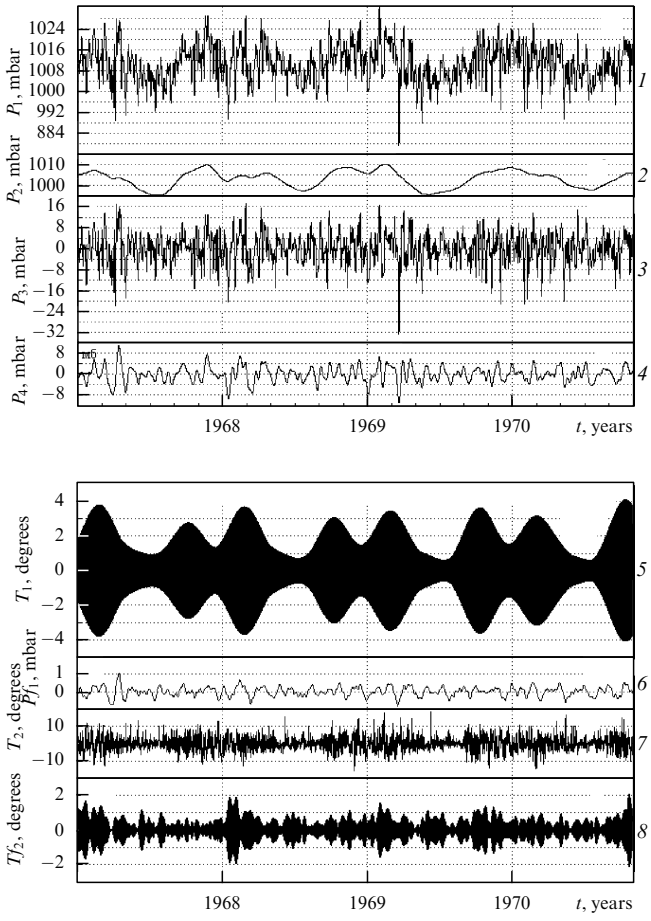

Figure 9. Comparison of variations in the atmospheric pressure $P(t)$ and temperature $T(t)$ at point Terneĭ: P_1, pressure variation; P_2, seasonal dynamics of pressure variations obtained by smoothing over a 60-day interval; P_3, deviations of pressure variations from the diurnal pattern; P_4, the result of smoothing the deviations of pressure variations over a 10-day interval; T_1, seasonal dynamics of daily temperature variations; P_f, deviations of the pressure variations predicted from the parameters of the 20 most intense narrow spectral lines in the range from 10 to 60 days; T_2, deviations of the daily temperature variations from the averaged seasonal pattern; T_f, predicted deviations of the daily temperature variations from the averaged seasonal pattern.

5.2 Fine structure of the diurnal spectral maximum in the air-temperature variations

In everyday life, a weather forecast is expected to predict impending rain, if any. A good predictor of rainy weather is the daily amplitude [31], or the temperature difference between the coldest and hottest hours of a given day. The daily amplitude depends on weather conditions. In calm, clear weather, it is twice that in cloudy and windy days. Therefore, changes in weather conditions modulate diurnal variations. The modulation in turn facilitates the formation of a fine spectral structure of temperature fluctuations in the vicinity of the narrow spectral line at a frequency of $DN = 2\pi$ day^{-1}, corresponding to a period of 24 hours.

Relatively slow synoptic and seasonal processes are manifest as a complicated spectral-line contour. If a process is strictly periodic and affects weather conditions, additional lines should appear in the vicinity of this line at combinations of the frequency DN and frequency harmonics of the process. In other words, the presence of a fine line structure in the spectral maximum of temperature variations at the frequency DN makes it possible to distinguish periodic processes that directly influence weather formation. The development of such a structure gives important evidence for the physical reality of oscillations responsible for the appearance of lines in pressure variation spectra.

This section reports the results of a study of the fine structure in the vicinity of the daily peak in the spectrum of temperature variations recorded at point Terneĭ in 1966–1984. The study analyzed consecutive air-temperature measurements at 0, 3, 6, 9, 12, 15, 18, and 21 h. As before, the quantity

$$Sy(\omega) = \left| \int y(t) \exp(\mathrm{i}\omega t)\, \mathrm{d}t \right|^2.$$

was used as the spectrum of function $y(t)$. The code allowed the spectrum to be computed from values averaged over a 6-h observation period. The data were recovered with a frequency resolution of 0.000392 day^{-1}.

Figure 10a shows the spectrum for point Terneĭ for a period of 5 years, from 1967 to 1972. The spectrum contains an intense line at frequency DN that corresponds to oscillations with a period of 24 hours and an amplitude of 2.56°, or a daily drop of 5.12°. A few additional peaks can be seen in the vicinity of this line, which have an approximately 10 times lower intensity. These peaks correspond to combination frequencies of daily variations with harmonics of a 1-year period. All other specific spectral features are virtually indistinguishable.

In order to illustrate the fine spectral structure, we subtract the averaged daily oscillations, whose parameters were estimated based on the main-peak phase and amplitude, from the temperature variations. The spectrum of variations with the diurnal harmonic subtracted is shown in Fig. 10b. The main part of the spectrum consists of seven almost equidistant lines. Their parameters, i.e. the period and amplitude, are presented in Table 7. The line frequencies coincide with the combinations $D-3S$, $D-2S$, $D-S$, $D+S$, $D+2S$, and $D+3S$ to the accuracy of unit resolution. The figure also shows other intense variations, the spectra of which are difficult to interpret. By way of illustration, purely periodic oscillations at the frequencies $D-4S$, $D-3S$, $D-2S$, $D-S$, $D+S$, $D+2S$, $D+3S$, and $D+4S$ with amplitudes and phases deduced from the spectrum in Fig. 10b were subtracted from the data of observations (Table 7).

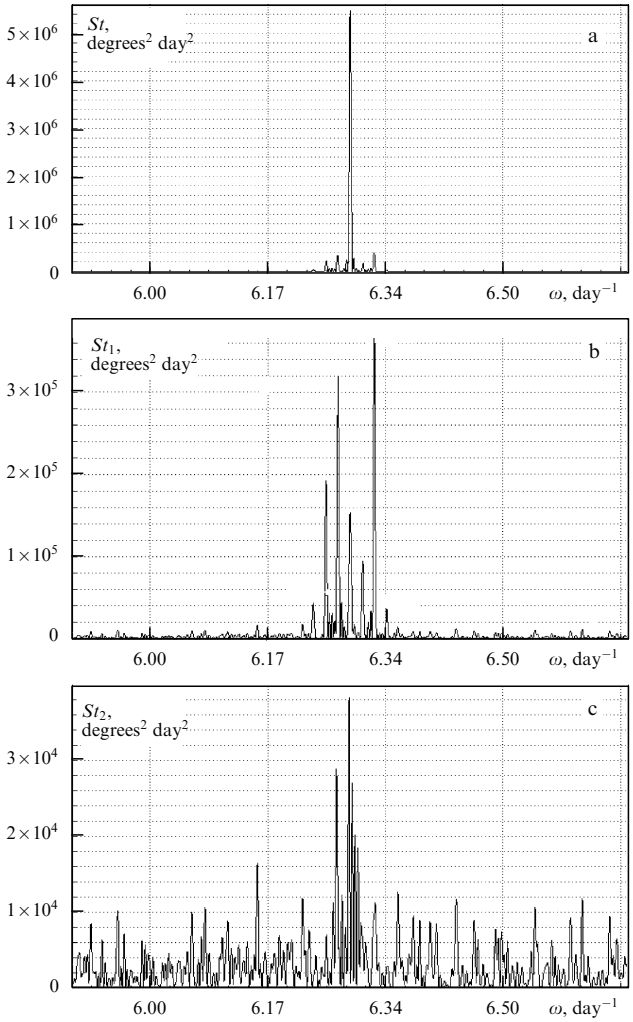

Figure 10. (a) Spectrum $St(\omega)$ of air temperature variations at point Terneĭ during 1967–1972 in the vicinity of the daily-variation frequency 2π. (b) Spectrum $St_1(\omega)$ after the subtraction of the periodic component corresponding to the parameters of the maximum at a frequency of 2π. (c) Spectrum St_2 of air-temperature variations after the subtraction of harmonics corresponding to the frequency combination of daily and yearly periods. The parameters of the lines are presented in Table 7.

The time variations of the subtracted oscillations are shown in Fig. 9 (graph *5*). These variations represent the averaged seasonal changes of the daily air-temperature drop at point Terneĭ. Spring and fall maxima are especially pronounced. Such representations can be used to compose long-term forecasts, which are, however, highly incomplete.

Table 7. Parameters of spectral lines at the combinations of the frequency of diurnal fluctuations and the harmonics of the 1-year period.

	Phase, rad	Period, day^{-1}	Amplitude, degrees
$D-3S$	−1.4042	6.2316	0.22359
$D-2S$	−1.4172	6.2492	0.52503
$D-S$	0.6570	6.2653	0.63580
D	0.7246	6.2830	2.56539
$D+S$	−1.4349	6.3015	−0.45818
$D+2S$	0.0831	6.3168	−0.68915
$D+3S$	−0.2569	6.3344	−0.20403

Variations that remain unpredicted are shown in Fig. 9, graph *7*. They are very significant.

The spectrum of the signal obtained after the subtraction of the averaged seasonal variations is shown in Fig. 10c. It contains pronounced spectral lines; in terms of amplitude, they are weaker than but comparable with the maxima of the seasonal-variation spectrum. The lines are of a very small width, which is in fact determined by the observation period chosen for analysis. The presence of such lines suggests the presence of long-term, strictly periodic processes, playing a role in weather formation. Their role is important. The strict periodicity of these processes shows promise of a substantial improvement in the accuracy of long-term weather forecasting. However, the objective of our study is not as ambitious as that. We wish to confirm that the strictly periodic processes responsible for the narrow maxima in atmospheric pressure spectra are the processes that cause changes in weather. For this purpose, we compare pressure-variation spectra and the fine structure of daily maxima in the spectra of atmospheric-temperature variations. The materials collected at point Terneĭ from 1967 to 1972 were used in our analysis.

5.3 Synoptic variability of atmospheric pressure and daily temperature variations

The variations of the atmospheric pressure at point Terneĭ (graph *1*) during 1967 – 1972 and their predictable fraction (graph *5*) are shown in Fig. 9. The same figure represents the seasonal dynamics of pressure variations obtained by smoothing over a 60-day interval (graph *2*). Weather (synoptic) variability is analyzed based on the deviations of the pressure variations from the seasonal pattern (graph *3*). The long smoothing interval (60 days) allows marked variations due to solar eclipses to be included in the analysis. We consider only variations with characteristic times of more than 10 days. In other words, the predicted dependence should be compared with the synoptic variation smoothed over a 10-day interval. This variable is shown in graph *4*. A comparison of this characteristic with the forecast based on spectral-maxima interpretation according to formula (32) (graph *6*) indicates that these variations can be predicted accurately in terms of both the time of appearance of maxima and minima (cyclones and anticyclones) and the amplitude (a forecast period of 4 years). Graph *5* in the same figure illustrates the seasonal dynamics of daily temperature variations obtained from the parameters of spectral lines at the combinations of daily fluctuations and harmonics of the period of 1 year (these parameters — phase, period, and amplitude — are presented in Table 7). A clear regularity in seasonal variations is evident: a rise in the atmospheric pressure correlates with a rise in the amplitude of daily temperature variations; a drop in the pressure is associated with a drop in the temperature.

Graph *7* in Fig. 9 shows the deviations of daily temperature variations from the averaged seasonal pattern. The largest deviations correspond to the passage of cyclones and anticyclones through the observation point manifest as the coincidence of the appearance of maxima and minima on the synoptic curve of atmospheric-pressure variations (graph *4*) with the maxima on the curve of deviations of daily temperature variations from the seasonal pattern (graph *7*).

Graph *8* illustrates the deviations of daily temperature variations from the averaged seasonal pattern predicted from 19 spectral maxima in the frequency range of $5.89 - 6.7\ \text{day}^{-1}$. The parameters of these lines are presented in Table 8. A comparison of graphs *7* and *8* indicates that such a prediction is less reliable than the prediction of atmospheric-pressure variations (graph *6*). Specifically, the time of weather anomalies can be predicted with a good accuracy, while the amplitudes of the predicted variations are several times smaller than the actual ones.

Table 8. Parameters of narrow spectral lines with the largest amplitudes.

No	Phase, rad	Frequency, day^{-1}	Amplitude, degrees
1	−0.5936	5.9154	−0.10206
2	1.0060	5.9535	−0.11169
3	−1.2831	6.0588	−0.11050
4	−0.0191	6.0772	0.10979
5	0.0457	6.1514	−0.13856
6	−0.6553	6.2151	−0.12876
7	0.3154	6.2504	−0.14811
8	−0.1093	6.2638	−0.27176
9	−1.3469	6.2826	0.44279
10	−1.0729	6.3011	0.24183
11	−1.2945	6.3148	0.20258
12	−0.4720	6.3513	0.12898
13	1.3498	6.3820	−0.10163
14	−0.9667	6.3965	0.10485
15	0.0642	6.4334	0.11917
16	1.1096	6.4585	−0.10308
17	0.1916	6.5449	−0.11068
18	1.5000	6.5956	−0.10552
19	0.2073	6.6121	−0.11858

Correlation between the variations of atmospheric pressure and the fine structure of the peak of daily temperature variations is even more evident when the spectra of these quantities are compared. The coincidence of the corresponding lines gives unambiguous evidence for the physical reality of the observed variations, since they lead to a real physical process — modulation of the daily temperature dynamics. The coincidence of the lines and spectral frequencies of solar eclipses indicates that the eclipses play an important role in weather formation on the Earth.

Figure 11a compares the fine structure of the daily temperature-variation spectrum and the spectrum of pressure variations with periods of 16 days or more. The zero point of the pressure spectrum falls on 2π; for lower frequencies, the spectrum is extended according to the rule $S(2\pi - \delta) = S(2\pi + \delta)$. Both spectra have a line structure composed of a large number of narrow lines. The width of individual lines is roughly 20 – 30 times smaller than the distance between them. The coincidence of lines is not complete. The coincidence is better illustrated by the curve showing the frequency dependence of the product of the spectra. In the case of coincidence, the line should be simultaneously present in both the spectrum and in the product of the spectra. An example of such a comparison is presented in Fig. 11b. Graph *1* shows the pressure-variation spectrum; graph *2*, the product of the pressure- and temperature-variation spectra. Coincident lines are pronounced, and their number is somewhat smaller than that of pressure-spectrum lines.

Not all lines in the spectra product are symmetric with respect to frequency 2π. There are more lines at lower frequencies. This means that not only fine-structure lines

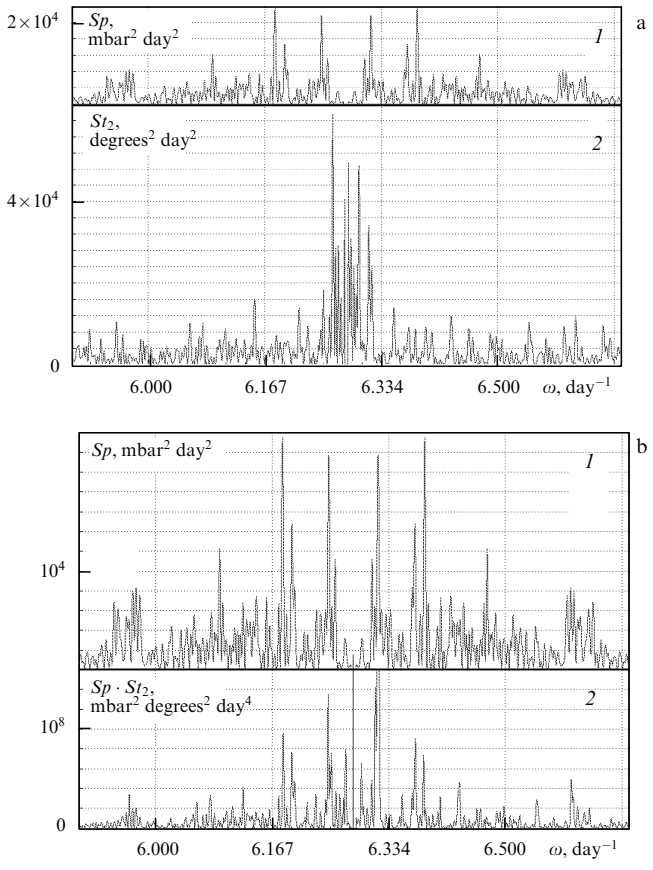

Figure 11. (a) Comparison of the atmospheric-pressure-variation spectra Sp for periods shorter than 16 days and the fine structure of the temperature-variation spectrum St_2 in the vicinity of a 1-day period (frequency 2π). The frequency axis for the pressure spectrum is shifted by 2π day^{-1}; (b) product $SpSt_2$ of the atmospheric-temperature- and pressure-variation spectra (graph *2*). Point Terneĭ, 1967–1972. The atmospheric-pressure spectrum Sp (graph *1*) is shown for comparison. \

produced by periodic processes but also fine-structure lines unrelated to the modulation of daily variations occur at frequencies from 5.8 to 6.28. Narrow lines at frequencies higher than 6.28 are of special interest in terms of a search for more convincing comparisons. They are interpreted as modulations of daily temperature variations by periodic processes. The modulation periods are 421, 210, 177, 161, 85.6, 71, 68, 60.6, 58, 49.2, 40.3, 35.0, 29.4, 28.6, 27.5, 25.9, 23.6, 22.03, 21.6, 19.9, and 16 days. Most of these lines are easy to recognize; in fact, they are lines of the spectrum of solar radiation perturbations caused by solar eclipses. Readily distinguishable are the lines corresponding to periods of 177 (0, 1), 85.6 (0, 2), 60.6 (1, −3), 58 (0, 3), 35.0 (1, −1), 30.0 (1, 0), 25.9 (1, 1), 22.0 (1, 2), 19.9 (2, −3), and 16.0 (2, −1) days. Figures in brackets are the line parameters from Table 6. Also observable are the lines with periods of 29.4 and 27.5 days, i.e. synodic and sidereal periods of the Moon. A more accurate location of the lines is impracticable for the reason that the length of the observation period is limited.

It can be concluded that periodic processes manifest as a line structure of atmospheric-pressure-variation spectra in a period range from 10 days to several years influence weather formation. This influence is apparent from the analysis of daily temperature variations in the form of a fine structure of their spectral peak in the vicinity of frequency 2π day^{-1}. It contains several series of spectral lines, with the main series formed by lines at frequencies of $i(M-S) \pm k(2S+2SAR)$ ($i = 0, \ldots, 4$, $k = \pm 1, 2, 3$) associated with solar eclipses. Lines fi in the spectrum of atmospheric-pressure variations (for periods from a few days to several months) are also visible in the temperature-variation spectrum at frequencies of $2\pi \pm fi$. Simulation of daily temperature variations based on the line parameters (phase and amplitude) allows the time of appearance and the magnitude of passing cyclones to be described for a period of 4 years with a resolution of 10 days.

This means that the observed lines in the atmospheric-pressure spectra are not merely fictions created by mathematical operations of spectrum construction but reflect real physical processes. Oscillatory processes manifest as sharp maxima in the spectra of atmospheric-pressure variations are real physical high-Q oscillations responsible for daily temperature fluctuations at the same frequencies. Therefore, variations in weather contain an intense purely periodic component, which can be predicted with a high degree of reliability for a few years in advance. It should be recalled that marked weather variations are attributable to the action of the Moon (solar eclipses).

6. Periodic climate variations

6.1 Introductory remarks

The presence of narrow lines in the spectra of atmospheric-pressure variations within a period range of 10–100 days permits predicting them several years ahead and thus knowing the time and magnitude of cyclones and anticyclones in advance which is of importance for long-term weather forecasting. Figure 10c shows that certain narrow spectral lines appear in the immediate vicinity of the daily peak of the air-temperature spectrum. They correspond to periods of modulating perturbations as long as 100 days or more. Such variations are of great importance for economic forecasting, e.g. in commercial fishing [31] and agriculture. Also, they are responsible for variations in biological activities. An example is provided by variations in the width of annual wood rings, shown in Fig. 12a (graph *1*). They correlate with variations in the mean annual temperatures (Fig. 12a, graph *3*, point Abashiri, the Sea of Okhotsk [32]) and variations in the thickness and lifetime of the sea-ice cover (Fig. 12a, line *2* [32]).

The time dependences of different characteristics have much in common. In order to select variations of common origin, Fig. 12b presents the spectra of variations in the width of annual rings, mean annual temperature, and total ice-cover area in the Sea of Okhotsk. If the spectra exhibit narrow lines, common sources can be revealed in the case where the positions of these lines in different spectra coincide. In order to eliminate effects of the ends of the observation interval on the structure of spectra being constructed, the results of smoothing over 50 years were subtracted from the variations of all parameters under consideration (variations with longer periods cannot be detected unless observations for more than 100 years are available; such variations are excluded from the analysis).

The spectra contain fairly narrow maxima, partly coincident for variations of different parameters. By way of illustrating coincident maxima, Fig. 12b compares the

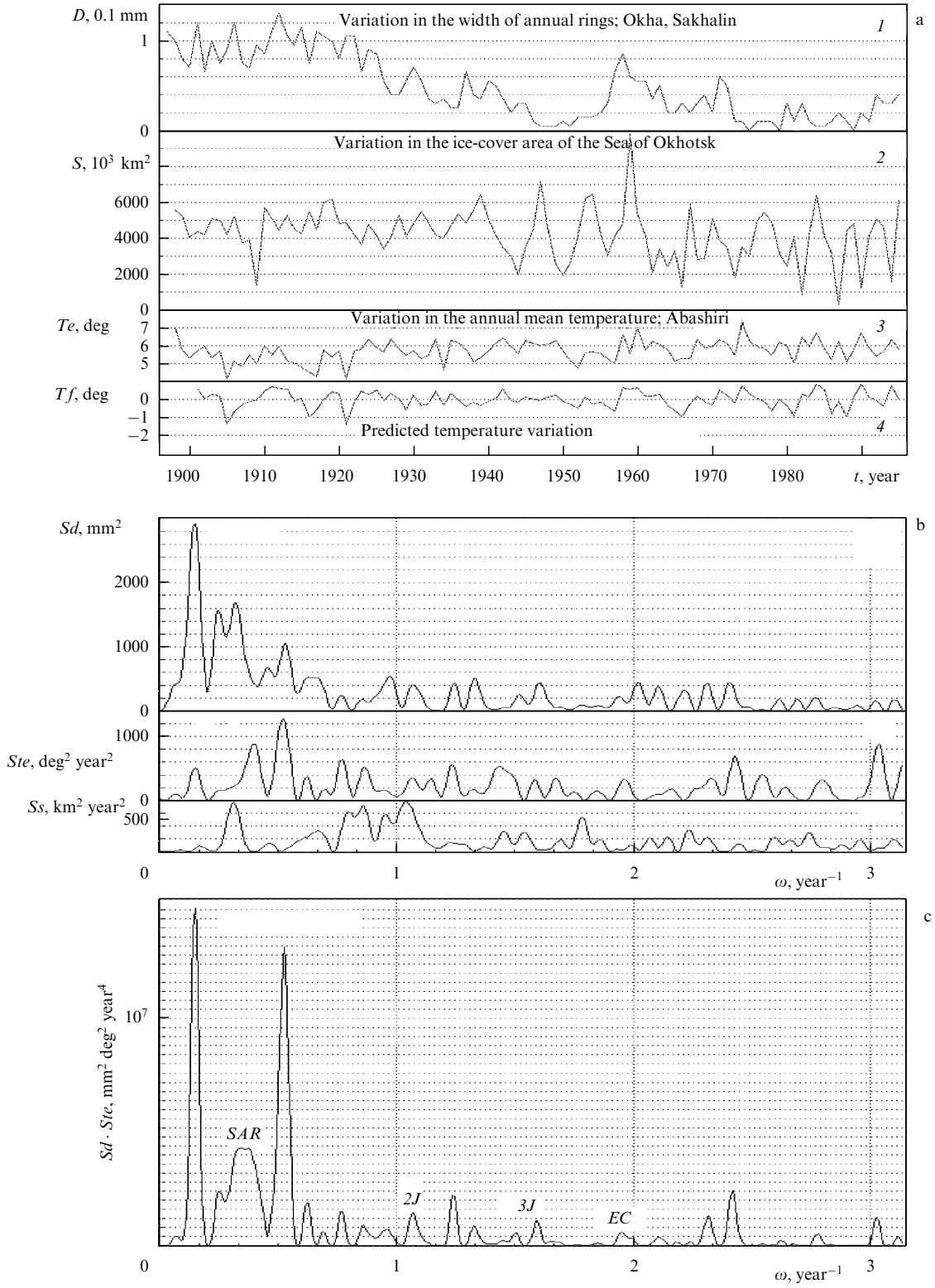

Figure 12. (a) Graph *1*: variations in the growth of wood (width of annual rings) D (M I Strel'tsov); graph *2*: maximum area of ice cover in the Sea of Okhotsk S [M Aota,1999]; graph *3*: changes in the mean annual temperature at point Abashiri Te [M Aota,1997]; graph *4*: predicted variations in the mean annual temperature at point Abashiri Tf based on a periodic representation. Time t is in years. (b) Spectrum of variations in the width of annual rings Sd, spectrum of the mean annual temperature at point Abashiri Ste, and spectrum of the maximum ice-cover area in the Sea of Okhotsk Ss. Frequency ω is in year^{-1}. (c) Product $Sd\,Ste$ of the spectra of variations in the annual-ring width Sd and the mean annual temperature Ste.

product of the spectra of variations in the annual ring width and the mean annual temperature. This procedure selects the lines whose maxima coincide from all others present in different spectra.

The figure demonstrates closely coincident and rather narrow maxima. The estimated corresponding periods are listed below. The largest maximum at low frequencies was ignored, since it results from the technical procedure of

subtracting the component smoothed over a 50-year-long period to eliminate the effects of the ends of the observation interval.

The periods estimated from the graphic representations are as follows: 25.0, 18.51 (SAR), 11.904 (J), 10.1, 8.13, 7.29, 6.53, 5.88 ($2J$), 5.07, 4.73, 4.16, 3.95 ($3J$), 3.21 (-1.6), 2.97 ($4J$), 2.71, 2.59, 2.26, 2.07 ($S-MR$) years. Some of these values are readily recognizable. These are the period of regression of the lunar orbital nodes (18.613), SAR; the period of Jupiter's revolution around the Sun (11.863), J; the periods of the first, $2J$ (5.93), second, $3J$ (3.952), and fourth, $4J$ (2.97), harmonics of Jupiter's rotation; the beating period of the solar-energy flux associated with eclipses (3.3) (the indices of the maximum are 1.6, in accordance with the notation in Table 6); and Mars' synodic period $S-MR$ (3.136). In the latter case, the coincidence of the periods is imperfect.

Periodic climate variations with the period of Jupiter's revolution have been discussed in the literature [33–35, 3]. It was assumed that they are due to oscillations of the Sun's center with respect to the center of gravity of the Sun–Jupiter system. Oscillations with the period of regression of the lunar orbital nodes were also addressed at scientific conferences [5] and attributed to variations in meridional convection due to inertial forces produced by the Earth's revolution around the common center of gravity of the Earth–Moon system. The relatively weak peak at a frequency of $-1.6 = 13S + 12SAR - M$ associated with variations in the solar illuminance during solar eclipses is a new finding. The physical meaning of other observed oscillations remains to be clarified, although some of the periods (5.07) were previously discussed in the literature [31].

A description of the periodic structure of climatic variations in this frequency range seems to be helpful for the analysis of climatic changes. Such an analysis is necessary in planning limitations on human activities, because periodic effects are much more pronounced than small anthropogenic temperature variations.

Estimates of peak phase and location may be used to forecast climatic fluctuations. The quality of such predictions is illustrated by Fig. 12a where graphs *3* and *4* serve to compare the variations in the mean annual temperature due to periodic changes (*4*) and the variations observed at point Abashiri. Evidently, the prediction is sufficiently accurate and no trend attributable to human activities can be revealed.

The positions of maxima with known periods can be used to interpret geological data. It was proposed [36] to trace catastrophes in Holocene deposits based on the dependence of the contact resistance on the depth of the deposit. Such measurements made by trivial methods on a section through a given deposit provide information about the properties of the section with a resolution of 1 mm. These measurements reveal marked quasi-periodic oscillations of resistance as a function of depth with periods of 2–6 cm. The spectrum of contact-resistance variations measured in Tserkovnaya Bay, Shikotan Island [36], is presented in Fig. 13. Two maxima are well defined (indicated by small black squares); the ratio of their positions is in fairly good agreement with the ratio of periods of the main maxima of climatic fluctuations (18.6 and 11.9 years). If such an interpretation of these maxima is true, it will be possible to determine the rate of deposit accumulation, rapidly and accurately estimate the age of geologic catastrophes identified using other signatures, and elucidate specific regional features of secular climatic trends [37] from the analysis of dynamic spectra of the series thus obtained.

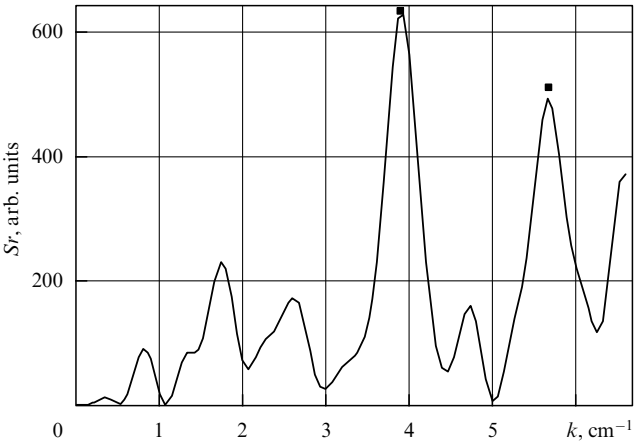

Figure 13. Spectrum $Sr(k)$ of contact resistance versus depth (cm^{-1}). Tserkovnaya Bay, Shikotan Island [32].

It can be concluded that the identification of spectral peaks in a period range of 2–50 years has important scientific and practical implications. Variations in the range from 100 days to 15 years will be subjected to a more detailed analysis below based on the data obtained during 40 years. The bulk of them are observations of sea-level fluctuations.

6.2 Spectra of sea-level fluctuations in a period range from a few months to several years

This section presents a detailed study of climate-variation spectra in the period range from 100 days to 15 years based on the spectral analysis of the simplest meteorological characteristic, sea-level fluctuations. In certain areas, they have been recorded for over 100 years. The choice of this parameter is dictated by the fact that we have at our disposal a very long series of relevant observations, from 1959 to 1990. The length of the series determines the frequency resolution that allows closely located lines to be reliably distinguished. However, this characteristic (sea-level fluctuations) is sufficiently interesting in itself. Its interpretation is employed in geology to study climatic changes on geologic time scales [3]. Today, certain authors try to use variations in the range of 5–40 years to study global warming [37]. True, it was shown that such studies need to take into consideration the contemporary Earth's motions and variations in the position of the detector fixation point related to earthquakes [6].

The analysis was made using data on sea-level fluctuation collected at the Tidal Research Station, Sakhalin Department of Hydrometeorological Service, point Kholmsk, Russia. The time dependence is presented in Fig. 14 (graph *1*). It represents sea-level fluctuations averaged over a 2-day interval. The component obtained by averaging over a 5-year interval is shown in graph *2* (Fig. 14). To construct the spectrum, it was subtracted from the original record.

The quantity $A(\omega) = \left|\sum Y(t_k)\exp(\mathrm{i}\omega t_k)\right|^2 \Delta t^2$ was computed, where t is the time from 1950 to 1990, Y represents the sea-level fluctuations after the subtraction of values averaged over a 15-year interval, $\Delta t = 2$ days, and ω is the cyclic frequency that varied over a range from 0.00785 to 15 year^{-1}. The spectrum is shown in Fig. 15 (line *1*).

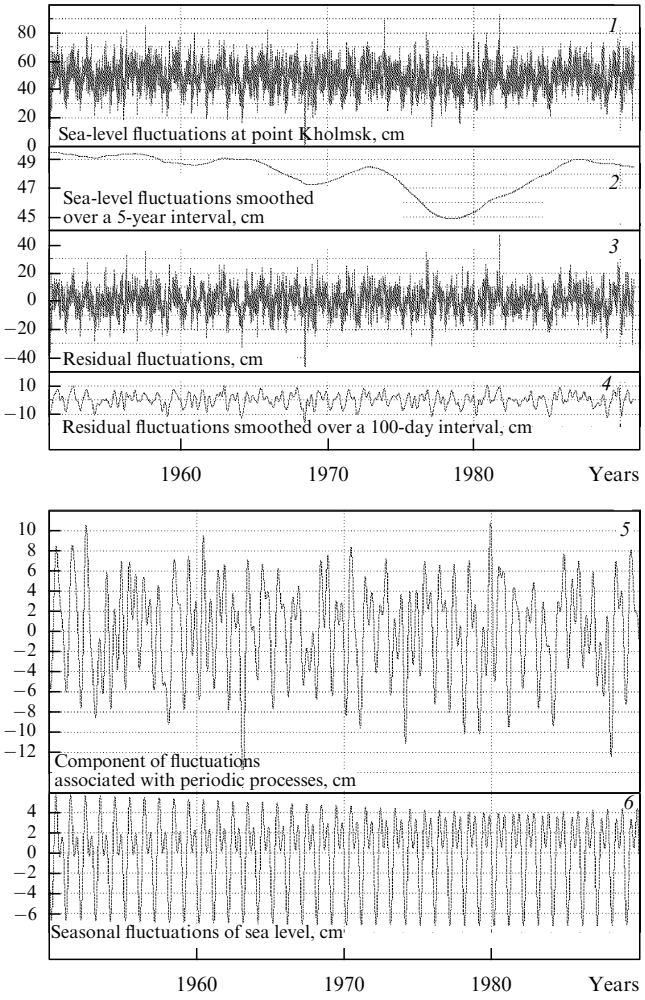

Figure 14. Sea level fluctuations at point Kholmsk: *1*, averaging over a 2-day interval; *2*, averaging over a 5-year interval; *3*, sea-level fluctuations with the 5-year average subtracted, used to analyze the spectrum; *4*, fluctuations to be compared, smoothed over a 100-day interval; *5*, estimate for these fluctuations based on the determination of seasonal variations and variations related to the changes corresponding to the spectral maxima listed in Table 9; *6*, seasonal fluctuations of sea level computed from the parameters of spectral maxima at frequencies S and $2S$.

The main feature of the spectrum is the presence of maxima corresponding to the periods of 1 year (S) and 0.5 year ($2S$). The former maximum is shifted by three sampling points. Fluctuations at these frequencies describe seasonal variations of the sea level. They have been examined in detail in Ref. [11] and are not included in the present study. Only one remark is in order. The main harmonic oscillations do not have a period of exactly 1 year, and the maximum is clearly displaced by a few sampling points. This displacement is manifest as beating in the oscillations of the fundamental and first harmonics, the frequency of which exactly corresponds to the period of 0.5 year. This beating is shown in Fig. 14 by line *6* and subtracted from the total spectrum.

The sea-level-fluctuation spectrum with the seasonal variations subtracted is presented in Fig. 15 (graph *2*). It has a line structure. The width of the majority of its lines depends on the duration of observations, which is indicative of purely periodic processes, neither the phase nor the period of which vary during this time.

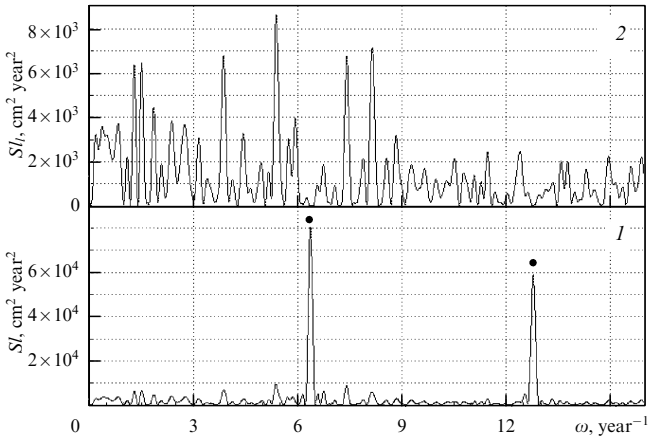

Figure 15. Spectra of sea-level fluctuations at point Kholmsk based on observations during 40 years: Sl, full spectrum (graph *1*); Sl_1, the spectrum after the subtraction of annual and semiannual variations determined from the parameters of the spectrum (graph *2*).

The periodic oscillations corresponding to the spectral maxima were computed and compared with the real sea-level fluctuations. The parameters of the maxima considered in the calculations are listed in Table 9. The periodic oscillations and the original dependence are compared in Fig. 14 (graphs *5* and *4*). The parameters of the lines taken into account are given in Table 9.

It can be seen that periodic oscillations contain the bulk of variations, and the evaluation of them from the parameters of spectral maxima yields a picture of sea-level fluctuations in a period range from 100 days to 15 years. In terms of quality, this description is no worse than that of tidal variations based on the Laplace theory [7], with use of the components corresponding to lunar and solar tides.

Thus, a large part of sea-level fluctuations observed in the period range from 100 days to 5 years are due to periodic processes, consist of individual harmonics, and can be predicted with a high degree of accuracy for many years in advance. The observed period values lie in a range character-

Table 9. Parameters of the lines for modeled sea-level fluctuations.

No	Phase, rad	Frequency, day^{-1}	Amplitude, deg
1	1.3273	0.0035	1.0845
2	−0.6092	0.0041	−1.0921
3	0.1101	0.0050	−0.9056
4	−1.1963	0.0064	−0.8407
5	0.2866	0.0074	0.8227
6	1.1171	0.0085	0.7548
7	−1.2680	0.0104	−1.1199
8	−0.3444	0.0120	0.7798
9	−1.3344	0.0145	−1.2635
10	−0.2516	0.0155	−0.7466
11	1.0314	0.0160	−0.8556
12	−1.3121	0.0200	1.1191
13	1.1990	0.0220	1.1483
14	0.0579	0.0238	−0.7709
15	0.8004	0.0250	−0.5852
16	−1.4966	0.0283	−0.6284
17	−0.5891	0.0309	0.6702
18	−1.3593	0.0334	−0.6742
19	−0.7892	0.0366	−0.6147

istic of combination frequencies of the orbital periods of the Earth, Mars, Venus, and Jupiter. In what follows, we will try to interpret the results of observations as a consequence of the action of planets. Three mechanisms of planetary action will be analyzed, all underlain by gravitational effects. One, the tidal action of planets on oceanic waters, was discussed in an earlier publication [7]. The second is associated with the gravitational action that planets exert on the orbit of the Earth – Moon system, shifting it towards the Sun. This shift results in a modulation of the solar irradiance, leading to a modulation of the atmospheric pressure and air temperature, which in turn causes sea-level fluctuations, in agreement with the inverted barometric law. The third mechanism is related to the modulation of periodic variations in the distance between the Earth and the Sun. It is analogous to the mechanism of line-*Mm* splitting in the lunar tidal potential, considered in Section 4. These mechanisms can be differentiated from one another by comparing the spectral-maxima amplitudes of sea-level and atmospheric-pressure variations. Such a comparison will be based on the interpretation of data on the atmospheric pressure collected at point Terneĭ over 18 years. Generally, this period is not long enough to reliably resolve all lines, but for some of them the results are more or less convincing.

6.3 Spectra of atmospheric pressure variations in the period range from 100 day to 5 years

This section presents the results of an analysis of the spectra of atmospheric-pressure variations (recorded at Terneĭ) in the period range from 100 days to 5 years. The objective of the study is to clarify whether these spectra have a linear structure similar to that discovered in sea-level-fluctuation spectra. Another objective is to estimate the fraction of the energy of variations contained in purely periodic components and prepare materials for a comparison with the linear structure of sea-level-fluctuation spectra in the given period range. As shown before, the ratio of amplitudes of the corresponding spectral maxima can be used to locate the primary perturbation in the atmosphere or in the ocean; moreover, it provides valuable information to be used in forming the concept of line origin.

Our analysis was based on the observations of atmospheric pressure at point Terneĭ during 1966 – 1984. The construction of spectra as described in Section 2 was employed as a method to identify periodic components. The spectra were constructed based on the signal smoothed over a 2-day period (graph *1* in Fig. 16) from which the secular variation (graph *2*) was subtracted. The secular variation was calculated as the result of smoothing the initial signal over a 5-year period. The spectra were computed from the residual variations remaining after the subtraction of the secular trend. They are shown by line *3*.

The spectrum was obtained at a frequency resolution of $\delta\omega = 2 \times 10^{-5}$ day^{-1}. It is presented in Fig. 17 (graph *1*). Its main elements are lines at periods of approximately 1 year (S) and 0.5 year ($2S$). These lines are much better noticeable than others, and minor details are poorly distinguishable. In order to reveal minor variations, the spectrum was constructed again after the subtraction of the seasonal component from the original series. This component was defined as the sum of sinusoidal components the parameters of which, i.e. amplitude, frequency, and phase, were found from the characteristics of maxima S and $2S$. The seasonal variations are shown by graph *6* in Fig. 16. Unlike sea-level fluctuations, atmospheric-pressure variations do not exhibit a marked deviation of maximum S from the frequency corresponding to a 1-year period. Moreover, the amplitude of maximum $2S$ is relatively small, which makes the secular variations of seasonal dynamics virtually imperceptible.

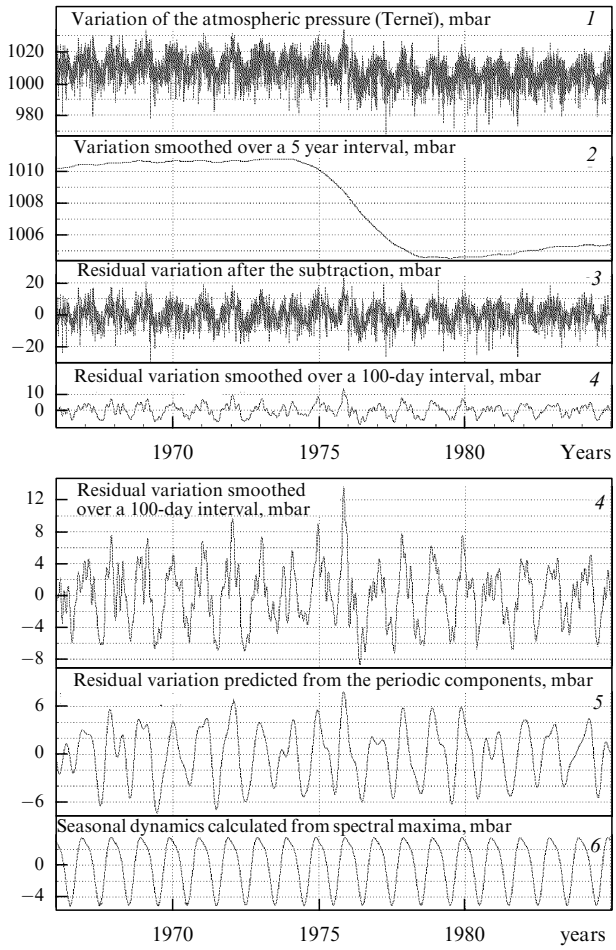

Figure 16. Variation of the atmospheric pressure at point Terneĭ in 1966 – 1984 smoothed over an interval of 2 days (graph *1*); secular trend of the atmospheric pressure variations at point Terneĭ (obtained by smoothing graph *1* over a period of 5 years); variation of the atmospheric pressure after the subtraction of the secular trend (graph *3*); the result of smoothing the subtracted variations over an interval of 100 days; variation of the atmospheric pressure predicted from periodic components in a period range from 100 days to 5 years (graph *5*). The lines considered and their parameters are listed in Table 11; the seasonal dynamics of the atmospheric pressure derived from the characteristics of spectral lines corresponding to periods of 1 year and 0.5 year (graph *6*).

The spectrum of variations after the elimination of the seasonal pattern is shown by graphs *2* and *3* in Fig. 17. The two graphs are used to illustrate the spectrum in view of the poor resolution attributable to the short observation period. Graph *2* is the spectrum of the signal with the seasonal variation subtracted. The spectrum contains several rather wide lines, but their number is significantly smaller than in a similar spectrum in Fig. 15 (graph *2*). Evidently, the interval of 18 years is too short to distinguish all lines. In order to see them, we tried to identify oscillations corresponding to the main maxima, eliminate them from the signal, and construct the spectrum again. The result is shown in graph *3*, which clearly exhibits additional lines missed on superficial examination of the spectrum.

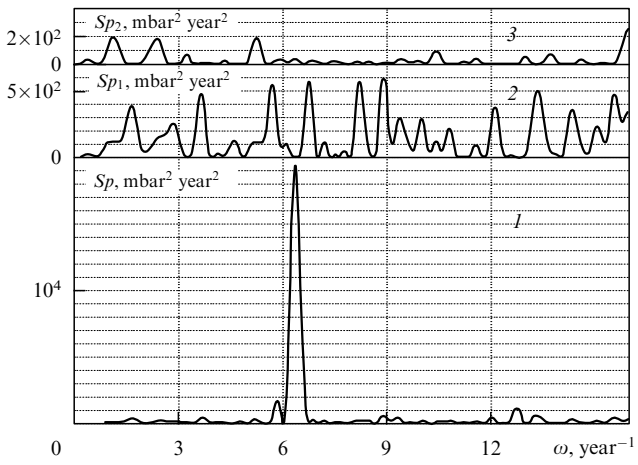

Figure 17. Spectrum of atmospheric-pressure variations at point Terneĭ *Sp*, calculated over a period from 1966 to 1984 in a period range from 150 days to 8 years (graph *1*): Sp_1, the spectrum of the signal after the subtraction of the seasonal component; Sp_2, the spectrum after the subtraction of the main maxima. Frequency ω is in year^{-1}.

Spectral components were calculated for the most intense lines whose characteristics are listed in Table 10. Their sum is shown in Fig. 16 (graph *5*). This quantity was obtained for the qualitative evaluation of the possibility to forecast variations in the atmospheric pressure from the parameters of their purely periodic components. Since only one line with periods in the range from 100 days to 5 years was used for the analysis, the result is compared to the pressure variation smoothed over an interval of 100 days. The latter is presented as graph *4* at two different scales. In the upper panel, it illustrates the fraction of variation energy that falls in the frequency range under consideration. Here, it is given on the same scale as the original series. In the lower figure, graph *4* is given on the same scale as the periodic component constructed from the spectral maxima to illustrate the fraction of energy contained in the purely periodic components of the signal.

It can be seen that the main part of the energy of atmospheric-pressure variations in a period range from 100 days to 5 years is associated with a purely periodic component. This important observation suggests that the given component can be predicted several years ahead with a a high accuracy.

To conclude, the spectrum of atmospheric-pressure variations in the period range from 100 days to 5 years has a line component containing the bulk of energy of all variations and can be predicted with a high accuracy for many years in advance.

Table 10. Parameters of lines in the spectrum of atmospheric-pressure variations at point Terneĭ.

No	Phase, rad	Frequency, day^{-1}	Amplitude, mbar
1	−0.5295	0.0044	−2.6076
2	1.5382	0.0077	3.9651
3	−0.3214	0.0098	−6.1437
4	1.4863	0.0124	2.8186
5	0.0811	0.0154	−6.3106
6	−0.1548	0.0183	−6.6586
7	0.4505	0.0195	−3.3586
8	1.3767	0.0223	−6.7872
9	0.3434	0.0241	−7.4833
10	0.1057	0.0252	−5.0085
11	−1.3481	0.0270	5.2369
12	−0.0992	0.0281	3.5963
13	−1.0536	0.0291	4.3310
14	0.8210	0.0312	2.6930
15	0.2987	0.0327	−5.2917
16	−1.2655	0.0361	7.0674
17	0.5163	0.0388	5.0434
18	−1.2618	0.0406	−4.3706

6.4 Spectral peaks of tidal potentials of Venus, Jupiter, and Mars

In what follows, we try to interpret the results of observations as an effect of planetary action. Three mechanisms are subjected to analysis, all underlain by gravitational effects. The first one, the tidal action of planets on oceanic waters, was discussed in an earlier publication [7]. The second is due to the gravitational action that planets exert on the Earth's orbit, shifting it towards the Sun. This shift results in a modulation of the solar irradiance, leading to modulations of the atmospheric pressure and air temperature, which in turn cause sea-level fluctuations, in accordance with the inverted barometric law. The third mechanism is related to the modulation of the periodic variation of the distance between the Earth and the Sun. It is analogous to the mechanism of line-*Mm* splitting in the lunar tidal potential considered in Section 4. The present section focuses on the first of these mechanisms. Theoretically, our analysis is nothing new. It is based on the Laplace theory [1] that regards the tidal-variation spectrum to be composed of a large number of thin lines at combination frequencies, which are combinations of harmonics of periodic motions of interacting planets. However, not all frequency combinations are equally intense. The energy distribution over different combinations depends on the mechanism of planetary action. The tidal-potential spectra of planets are presented below, but only the tidal-potential spectrum of Venus is described at length. The spectra of Mars and Jupiter were examined in a similar manner.

Our theoretical analysis of sea-level fluctuations ζ was performed using the Newton formula slightly modified to take into account certain simplifications arising from the concrete parameters of the Venusian orbit [15, 16]:

$$\zeta = \frac{(3/2)\,\sin^2\varepsilon\,(\cos^2\theta - (1/2)\,\sin^2\theta)\,(V/E)\,(a/R_S)^3}{\left(1+\alpha^2-2\alpha\,\cos(\omega_V t-\Phi-\omega_E t)\right)^{5/2}} \times a\left[\cos^2\omega_E t+\alpha^2\,\cos^2(\omega_V t-\Phi) - 2\alpha\,\cos(\omega_V t-\Phi)\,\cos\omega_E t\right], \quad (33)$$

where $\omega_E = 2\pi$ year^{-1} is the frequency of the Earth's revolution around the Sun, $\omega_V = 10.23$ year^{-1} is the orbital-revolution frequency of Venus, $\Phi = -0.04$ is the phase of motion of Venus in January 1950, $\alpha = R_V/R_S = 0.723$ is the ratio of orbital radii of Venus R_V and the Earth R_S, $V/E = 0.817$ is the mass ratio of Venus and the Earth, a is the Earth's radius, $\varepsilon = 23°27'$ is the inclination of the Earth's equator, and θ is the latitude of the observation point.

The spectra were constructed for a period from 1950 to 1990 using formula (33). The spectral amplitude was found to be 0.018×10^{-4} cm^2 year^2 and correspond to a sea-level-fluctuation amplitude of $\sim 10^{-5}$ cm. The spectrum is shown in Fig. 18a (graph *1*).

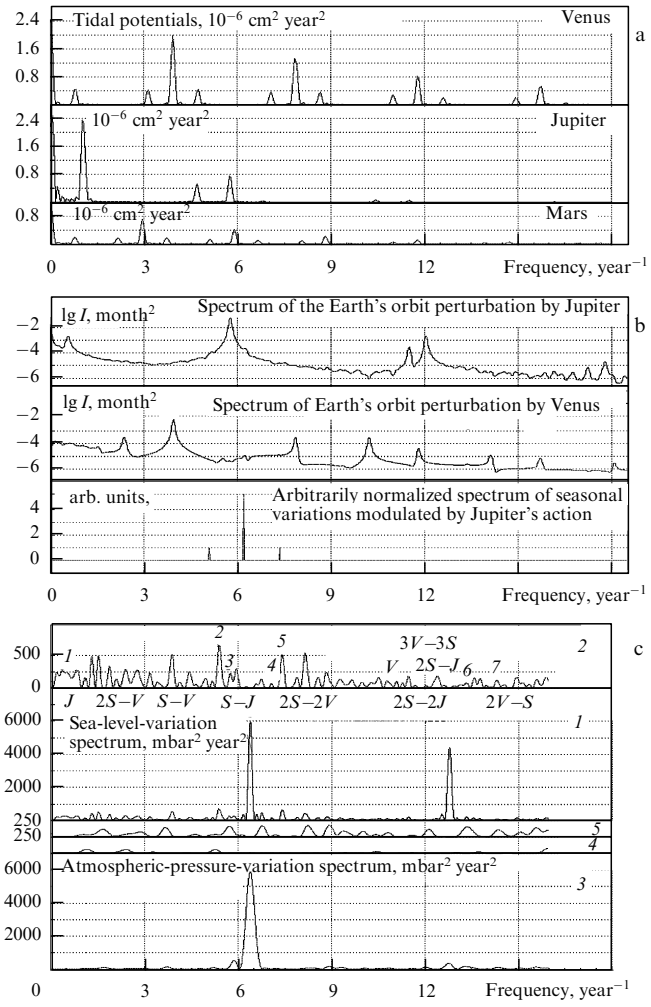

Figure 18. (a) Tidal-potential spectra of Venus, Jupiter, and Mars. (b) Spectra of the relative radial perturbations of the Earth's orbit by the gravitational action of Jupiter and Venus and an arbitrarily normalized representation of the seasonal-variation spectrum perturbed by the Jupiter-induced modulation of radial oscillations. (c) Spectra of sea-level fluctuations at point Kholmsk (graphs *1*, *2*) and atmospheric-pressure variations at point Terneĭ (graphs *3*, *4*). Graphs *2*, *4*, and *5* represent the spectra obtained after the subtraction of the seasonal variations.

It can be seen that the spectrum of the Venusian tidal potential contains several bands, each split into three lines. The central line of each band is characterized by a maximum intensity and has the frequency of one of the harmonics of the synodic period (583.92 days, or 1.598 years). Side lines are located at a distance of $\Delta_V = 0.798$ year^{-1}. The frequency Δ_V is a combination of the frequencies of orbital revolution of Venus ($\omega_V = 10.213$ year^{-1}) and Earth ($\omega_E = 6.2830$ year^{-1}) around the Sun, equal to $5\omega_E - 3\omega_V$.

The same Fig. 18 shows the main lines of the tidal-potential spectra of Jupiter and Mars. The spectral structures of Jupiter and Venus are markedly different because the orbital radius of Jupiter is considerably larger than that of the Earth, while variations in the distance between these planets are much smaller compared with the distance itself; hence, the intensities of higher harmonics are small. The maximum spectral line of Jupiter corresponds to the second harmonic of the period of its revolution around the Sun (Jupiter's frequency is $\omega_J = 0.5297$ year^{-1}, and the period of the first harmonic is $4\pi/\omega_J = 5.931$ years). The intensity of this line is approximately 10 times lower than that of the strongest Venusian lines. The amplitudes of oscillations at certain combinations of frequencies ω_J and ω_E, i.e. $\omega_E - 3\omega_J$, $\omega_E - \omega_J$, and $\omega_E + \omega_J$, are also large. Other combinations are weaker in the ratio of $(D/R_J)^2 = 0.037$; R_J is Jupiter's orbital radius.

The strongest lines of the Martian tidal potential are almost ten times less intense than those of Venus, but also contain a sequence of bands each composed of three lines. The central line of each band is the most intense, and its frequency coincides with a harmonic of the Martian synodic period T_M ($T_M = 780$ days, $\omega_M = 3.336$ year^{-1}). Side lines in individual band are much less intense and lie $\Delta_M = 4\omega_M - 2\omega_E = 0.78$ year^{-1} apart. It should be noted that $\Delta_M \cong \Delta_V$, and the frequencies of some intense lines in the spectra of Mars and Venus are very close and poorly resolvable, as in the case of Jupiter and Venus.

Theoretical estimates for the main spectral lines of tidal potentials are given for comparisons with the observed ones.

6.5 The theory of planetary-motion-induced variations in solar irradiance

The tidal force is not the sole source of sea-level perturbations at combinations in the frequencies of revolution of the Earth and other planets around the Sun. A certain perturbation is due to variations in the Earth's orbit under the action of planets resulting in a change of the distance between the Earth and the Sun. This change accounts for an alteration in the total solar irradiance at the Earth. The mechanism of these perturbation is illustrated below by the example of the influence of Venus.

Figure 19 is a schematic representation of the motion of this planet and the Earth around the Sun, positioned at the origin of the system of coordinates. Plane X, Y coincides with the plane of the Earth's orbit. Points E_0 and E_1 are the Earth's positions at the initial time of analysis (1 January 1950) and at a certain intermediate point t. Points V_0 and V_1 are the positions of Venus at the beginning of the analysis (1 January 1950) and at a certain intermediate point t. We denote the angle between the orbital planes as γ. It is assumed to be small and taken equal to zero for the preliminary estimate.

The distance r between the planets is

$$r = \left(R_S^2 + R_V^2 - 2R_S R_V \cos(\Phi_1)\right)^{1/2}. \qquad (34)$$

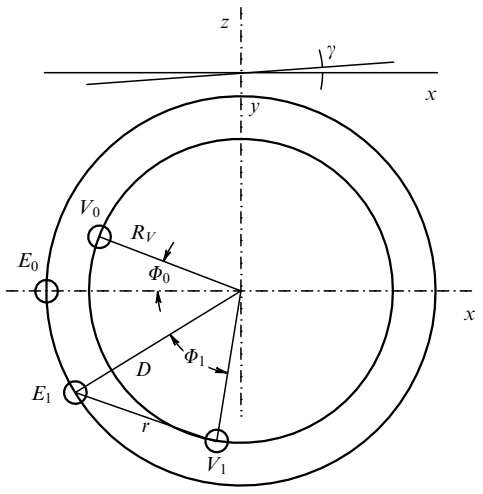

Figure 19. Schematic representation of motions of the Earth and Venus.

Here, R_S and R_V are the orbital radii of the Earth and Venus, Φ_1 is the angle between the directions to the Earth and Venus from the origin of coordinates, $\Phi_1 = \omega_V t - \Phi_0 - \omega_E t$, $\omega_E = 0.523\ \text{month}^{-1}$ is the Earth's orbital frequency, $\omega_V = 0.8511\ \text{month}^{-1}$ is the orbital frequency of Venus, $\Phi_0 = -0.04$ is the phase of motion of Venus in January 1950, and the angle $\gamma = 3°23'38.9''$ is small and taken to be zero hereafter.

The gravitational force A acting from Venus on the Earth is directed along the line E_1V_1 and equals $A = fM_V M_E/r^2$; $M_V = 0.878\ M_E$ is the mass of Venus, and $f = 6.7 \times 10^{-8}\ \text{cm}^2\ \text{g}^{-1}\ \text{s}^{-3}$ is the gravitational constant.

Perturbations of the solar energy flux occur as the Earth moves to the Sun, in proportion to the quantity $-2l/R_S$, where l characterizes the Earth's displacement toward the Sun. It depends on the component of force A in the direction to the Sun, $(fM_V/r^2)\cos\delta$. The angle δ between the directions to the Sun and Venus can be found from the equation $R_S^2 + r^2 - 2R_S r\cos\delta = R_V^2$.

The radial displacement of the Earth toward the Sun is given by the equation

$$\frac{\mathrm{d}^2 l}{\mathrm{d}t^2} = \frac{fM_V(R_S^2 + r^2 - R_V^2)}{2R_S r^3}\,. \tag{35}$$

The time dependence on the right-hand side of this equation is related to r. It is a periodic dependence with the Venusian synodic period $T_V = 2\pi/(\omega_V - \omega_E) = 583.92$ days. In order of magnitude, the displacement l is

$$l = \frac{fT_V^2}{(2\pi)^2 M_E} = \frac{gT_V^2 a^2 D}{(2\pi)^2 (D - R_V)^3}\,\frac{M_V}{M_E} \sim 10^4\ \text{km}\,;$$

where g and a are the acceleration of gravity ($9.8\ \text{m s}^{-2}$) and the Earth's radius (6,370 km), respectively. Such displacements can induce temperature variations $\sim 2l/(D\,T_0) \sim 0.3°$ and atmospheric-pressure variations of ~ 1 mbar, ($T_0 = 300°$ is the mean temperature at the Earth's surface). The latter value is in good agreement with the estimated variations of pressure.

The orbit-perturbation spectrum (35) contains only lines at harmonics of the planetary synodic period; the line with a minimal period corresponds to a maximum energy. The amplitude of the first harmonic is 20 times smaller than that of the zeroth harmonic.

The frequencies of the observed perturbations do not satisfy this condition even if only oscillations primarily generated in the atmosphere are taken into consideration. Oscillations at combination frequencies can occur as a result of the Earth's rotation about its axis, its most prominent effect being a restricted energy exchange between the Northern and Southern hemispheres. Variations in the energy flux coming to one hemisphere need to be considered to estimate perturbations at combination frequencies. This leads to an additional variation in the solar-energy flux with a period of 1 year. In this case, the energy incident on the northern hemisphere is

$$\frac{1}{2}\left(1 + \sin E \cdot \cos(St + \Phi_l)\right);$$

where Φ_l is the phase of the Earth's revolution around the Sun. This modulation taken into account, the spectrum contains additional lines at frequencies $k(\omega_V - \omega_E) \pm \omega_E$. Since spectral lines are substantially different in terms of intensity, the spectrum is presented in Fig. 18b on a logarithmic scale. Analogous data for Jupiter are also shown in the same figure.

It is worthwhile to note that perturbations of the Earth's motion around the Sun due to Venus are not as great as those caused by Jupiter. The effect is proportional to the planet's mass and the square of the period but inversely proportional to the square of the minimal distance between the planets. In other words, the relative contribution of Venus compared with that of Jupiter is

$$\frac{V}{J} = \frac{M_V}{M_J}\left(\frac{R_J}{R_S - R_V}\right)^2\left(\frac{T_V}{T_J}\right)^2 = 10^{-3}\,.$$

This ratio holds for the fundamental harmonic of Jupiter. In the analysis described above, only secondary harmonics were examined, which are weaker by a factor of $R_S/R_J = 0.2$. This means that the main lines of Venus and secondary lines of Jupiter have comparable amplitudes, and the action of both planets should be taken into consideration in the analysis of the physical nature of the observed spectral lines of sea-level fluctuations.

The lunar action produces a similar effect, but the description needs to be somewhat more complicated. Precession leads to oscillations of the center of mass of the Earth – Moon system with respect to an elliptical orbit. These oscillations have a period of 18.61 years and an amplitude of $\Delta_S = D\,M/E = 4700$ km. They occur in the plane tilted by 5° from the the orbital plane, that is virtually in the Earth's orbital plane. The effect of these oscillations is comparable with that of Jupiter. They should also be regarded as a source of perturbations on lines SAR and $S + SAR$.

6.6 Modulation of the Earth's radial-oscillation frequency

An analysis of lunar tides related to oscillations of the Moon's orbital radius (line Mm) revealed a marked effect of the Sun on the spectrum formation, which is responsible for the difference between the periods of oscillatory and rotational motion of the Moon (see Section 4.2). A similar effect can be observed in the Sun – Earth system, which undergoes analogous perturbation by the action of the planets. For remote planets, such as Jupiter, the perturbation period considerably exceeds the period of the Earth's orbital motion; therefore, the perturbation can be regarded as adiabatic. In this case, the perturbation effect is determined by the parameter

$$\alpha_J = \frac{M_J}{M_S}\left(\frac{R_E}{R_J}\right)^3 = 0.66 \times 10^{-5}\,,$$

where M_J and M_S are the masses of Jupiter and the Sun, respectively, and R_E and R_J are the orbital radii of the Earth and Jupiter. The effect creates the difference the difference

$$\delta\omega_J = -1.75\alpha\omega_E = -0.19 \times 10^{-6}\ \text{day}^{-1}$$

between the frequencies of radial oscillations and rotation of the Earth and to modulates the radial oscillations with a modulation frequency equal to the doubled frequency of Jupiter's revolution $2\omega_J$ with a modulation amplitude $\delta\omega_{J1} = (3/8)\alpha\omega_E$. The latter accounts for the broadening of the spectral line corresponding to the radial-oscillation frequency and for the appearance of additional lines at $\omega_{Jk} = S \pm 2k\omega_J$. Here, ω_E and ω_J are the orbital frequencies of the Earth and Jupiter. When $\delta\omega_{J1}\,T \ll 1$, the amplitude of

the additional lines with index k (k is an integer) is proportional to $(\delta\omega_{J1}T)^{2k}/(k!)^2$. In other words, lines with large k have small amplitudes; virtually, only two additional lines appear at frequencies $\omega_{J1} = S \pm 2\omega_J$.

The substitution of the known characteristics of Jupiter and $T = 40$ years (used for the construction of spectra) gives $\delta\omega_{J1}T \sim 10^{-3}$ and a difference between the periods of the Earth's radial oscillations and rotation of $\delta T \cong 0.004$ day. This value is smaller than that obtained by astronomers [18], who accept the values of 365.242 and 365.2596 days for the revolution period TE1 (tropical year) and the period of radial oscillations (anomalistic year), respectively. This is quite natural, since not only Jupiter controls the difference between the periods. Other planets can exert a similar influence, and their effects are added.

Thus, the modulation of oscillation frequencies of the Earth's orbital radius under the action of planets should produce spectral lines in the vicinity of the peak corresponding to a period of 1 year, at distances $\pm 2\omega_\gamma$ from this peak (γ denotes planets — Mars, Jupiter, Saturn, etc.). The intensity of these lines is proportional to the parameter $\alpha_\gamma = M_\gamma/M_S\,(R_E/R_\gamma)^3$, where M_γ and R_γ are the mass and the orbital radius of a planet, respectively. Generally speaking, these estimates hold only for the case of $(R_E/R_\gamma) \ll 1$. However, the use of such an estimate for the analysis of planetary effects indicates the leading role of Jupiter, Venus, and Mars. The order of magnitude of the ratio of intensities of these lines to the intensity of the maximum at frequency S is determined by $(\delta\omega_{J1}T)^2$. If the known estimate of $\delta\omega_{J1} = 0.00029$ year^{-1} is true, then the intensity of these lines in the spectra constructed for an observation period of 40 years is more than four orders of magnitude smaller than the peak intensity at S.

It should be noted that the modulation of the period of oscillations of the distance between the Earth and the Sun is due to the precession of the lunar orbit. The Moon's precession gives rise to variations in the distance between the center of gravity of the Earth – Moon system and the Sun with a period of 18.61 years (corresponding to SAR). As a result, the potential energy changes; this leads to an increase in the period and a modulation of the radial-oscillation frequency. The modulation occurs with a frequency of $2SAR$ and has an amplitude of $\delta\omega_{SAR} = \omega_2\Delta_S/R_S$. In the spectrum, it is manifest as additional lines at frequencies $S \pm 2SAR$ with an amplitude proportional to $\delta\omega_{SAR}T = 10^{-3}$ and comparable with a similar effect produced by Jupiter.

6.7 Analysis of the observed spectral lines of sea-level fluctuations

An analysis of the nature of the observed spectral lines confirms their reality and the possibility of using them for reliable forecasting of climatic variations. Therefore, such an interpretation may have some practical implications. Among the theories reviewed in this paper, only the theory of modulation of the solar radiation due to the Earth's orbital oscillations under planetary action (mechanism A) estimates the variations to be comparable with the observed values in terms of spectral-maxima amplitudes. Other theories (the tidal theory and the theory of frequency modulation of radial motion) yield estimates differing by several orders of magnitude from the real values. Sea-level fluctuations estimated based on the theory of gravitational tides (mechanism C) and the theory of frequency modulation (mechanism B) differ from the actual values by four and two orders of magnitude, respectively. Therefore, the interpretation of a line as an effect of the action of mechanism A appears preferable. These preferences were used here to interpret spectral lines. All the above mechanisms lead to line-structured spectra at combinations of the frequencies of revolution of a given planet and the Earth around the Sun. However, each mechanism is characterized by specific-energy distribution patterns among the spectral lines. For this reason, certain lines cannot be interpreted in terms of the action of mechanism A, and their appearance has to be explained on the assumption that mechanism B is an underlying cause.

Table 11 shows spectral-line parameters interpreted to be attributable to mechanism A. Lines numbers are given in the first column; the second one presents the frequency combinations at which the spectral maxima occur; the third, the theoretical values of the corresponding periods estimated from astronomical data (years); the fourth, the logarithms of the maximum amplitudes (units/month^2); the fifth, the periods calculated from the positions of maxima in sea-level-fluctuation spectra (years); the sixth, the logarithms of the ratios of the spectral-maximum amplitudes to the amplitude at a period of 1 year; and the seventh, the logarithms of the ratios for the maximum amplitudes in atmospheric-pressure-variation spectra. The interpreted maxima are presented in Fig. 18c. The maximum at frequency SAR cannot be analyzed because of the low quality of interpretation for such long periods.

The data in Table 11 demonstrate a good agreement between the periods, which could not be better, given the observation period of 40 years. However, the maximum amplitudes in the spectra of sea-level fluctuations are one order of magnitude higher than the estimated ones, although, theoretically, they should be lower. Moreover, there are many lines at frequencies coincident with combinations of planetary revolution frequencies, which should not be observed according to theory. This refers in the first place to the line at frequency $S + 2J$, the strongest one in the sea-level-fluctuation spectra. This line is symmetric to a maximum at frequency $S - 2J$ with respect to line S. This is a result of the periodic influence of Jupiter on the Earth's orbit with a period of $2J$. This interaction was analyzed in the preceding section and should result in the appearance of lines at frequencies $S \pm 2J$ with an intensity four orders of magnitude lower than that of line S. Both lines are actually observed, but their

Table 11. Spectral lines interpreted in terms of model A.

No	Parameters of frequency combination	Theoretical estimates for the line: 1, period (years); 2, logarithm of amplitude		Spectral lines of sea-level variations: 1, period (years); 2, logarithm of amplitude		Logarithm of pressure-spectrum amplitude
1	2	1 (3)	2 (4)	1 (5)	2 (6)	7
1	J	11.86	−2.51	11.83	−1.90	
2	$2S-V$	2.673	−3.28	2.686	−1.3	−1.98
3	$V-S$	1.599	−1.84	1.63	−1.1	−1.79
4	$S-J$	1.092	−1.04	1.089	−1.33	−1.03
5	$S+SAR$	0.946	—	0.945	−1.09	—
6	$2V-2S$	0.7995	−3.27	0.809	−1.4	−1.94
7	V	0.6152	−3.26	0.618	−1.79	−1.30
8	$2S-2J$	0.546	−3.35	0.545	−2.125	−1.96
9	$3V-3S$	0.533	−4.01	0.531	−2.16	−1.8
10	$2S-J$	0.522	−2.47	0.518	−1.66	−1.73
11	$2V-S$	0.442	−5.075	0.440	−2.4	−1.73

relative intensities are 0.116 and 0.107 respectively, i.e. two orders of magnitude higher than the theoretical values.

Such a discrepancy agrees with the observed difference between the periods of the Earth's radius oscillations (line S) and orbital motion (double period of line $2S$). The theoretical difference between these periods is 0.017 day, which should virtually not be observed. However, this effect is actually observable as pronounced variations in the seasonal dynamics shown in Fig. 14 (graph *6*). The real values obtained by the interpolation of the derived spectral characteristics are as follows: the radial-oscillation period is 365.89 days, and the period of revolution is 364.98 days. A difference of 1 day between the periods is near the limit of resolution in the analysis of a 40-year-long observation series (the actual limit of resolution is 0.5 day). It can therefore be concluded quite reliably that the theory underestimates the effect. If so, the relative spectral amplitudes of the additional lines at planetary periods of $S \pm 2\omega_\gamma$ are also underestimated; in fact, they should be about two orders of magnitude smaller than the maximum amplitude at S. The corresponding lines can be observed in real spectra. Their characteristics are listed in Table 12.

Table 12. Spectral lines interpreted in terms of model B.

№	Parameters of frequency combination	Theoretical estimates for the line: 1, period (years); 2, logarithm of amplitude		Spectral lines of sea-level variations: 1, period (years); 2, logarithm of amplitude		Logarithm of pressure-spectrum amplitude
1	2	1 (3)	2 (4)	1 (5)	2 (6)	7
1	$2M-S$	15.79	−3.56	15.39	−1.35	−2.7
2	$S-2J$	1.202	0.708	1.192	−0.93	−2.05
3	$S-2SAR$	1.120	—	1.119	−1.35	−1.67
4	$S+2SAR$	0.903	—	0.903	−1.54	−2.08
5	$S+2J$	0.8557	−0.708	0.861	−0.97	−2.3
6	$S+2M$	0.484	−3.56	0.486	−2.03	−1.82
8	$2V-S$	0.442	0.668	0.440	−2.04	−1.73

Table 12 shows spectral-line parameters interpreted to be attributable to mechanism B. The first column contains line numbers; the second one, the frequency combinations at which the spectral maxima occur; the third, the theoretical values of the corresponding periods estimated from astronomical data (years); the fourth, the logarithms of the ratios $(M_\gamma/M_E)^2\,(R_E/R_\gamma)^6$ theoretically proportional to the spectral-maximum amplitude; the fifth, the period values calculated from the positions of maxima in sea-level-fluctuation spectra (years); the sixth, the logarithms of the ratios of the spectral-maximum amplitudes to the amplitude at a period of 1 year; and the seventh, the logarithms of the ratios for the maximum amplitudes in atmospheric-pressure-variation spectra. The interpreted maxima are presented in Fig. 18c.

The data in Table 12 demonstrate good agreement between the periods. However, the amplitudes of the maxima in the spectra of sea-level fluctuations do not agree quite well with those found theoretically. The largest difference is observed in the case of line No 1 because it occurs against the background of the strong line corresponding to a period of SAR (18.613 years). The table also includes two lines with periods of $S \pm 2SAR$. They result from the modulation of the period of oscillations in the distance between the Sun and the Earth associated with the regression of lunar orbital nodes. These lines are clearly seen in the spectrum. A part of the spectrum of sea-level fluctuations after the subtraction of seasonal variations in the vicinity of line S is shown in Fig. 20.

Figure 20 illustrates the positions of the identified lines. Evidently, most of the observed intense lines find a rational interpretation based on theoretical estimates considered in the previous sections. Positions of minor maxima can be interpreted if the positions of lines associated with tidal potentials are included in the analysis. By way of example, line $3M-3S$ of the Martian tidal potential is distinguished in Fig. 20. Its intensity is several orders of magnitude higher than the theoretical value. However, certain strong lines fail to be interpreted. One of them is labeled by a question mark. In other words, the interpretation of spectral lines remains an object of investigation. This, however, should not obscure the main fact that the lines are a physical reality describing periodic climatic variations; the phase and the amplitude of the lines can be used for long-term forecasting of climatic changes.

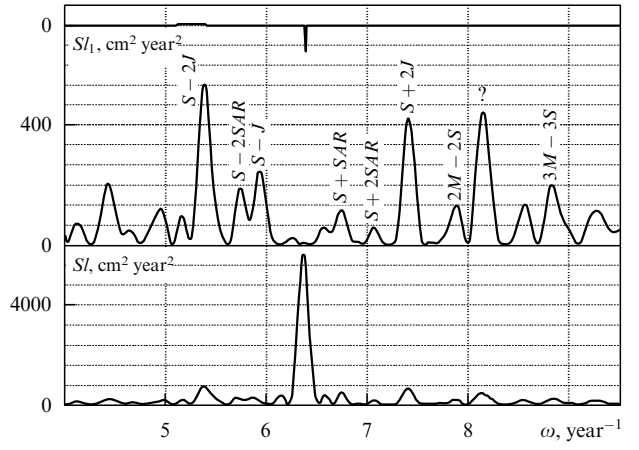

Figure 20. Spectrum Sl_1 of sea level fluctuations, with the seasonal variations subtracted in the vicinity of the peak corresponding to oscillations with a period of 1 year. The lower line shows the spectrum prior to the subtraction of the seasonal component Sl. Frequency ω is in year^{-1}.

Although our primary objective was to prove the reality of periodic climate variations, the study revealed in parallel the interesting physical fact that there are marked differences between the periods of the Earth's orbital revolution and oscillations in the distance between the Earth and the Sun. Both these phenomena should contribute to the formation of line S, which therefore should consist of two complex peaks, resembling line Mm related to the lunar motion. This suggests that the analysis of spectra of sea-level fluctuations over periods of 100 and 200 years may be instrumental in resolving the components of this peak and accurately determining the period of radial oscillations, the evaluation of which by astronomical methods is of dubious accuracy.

7. Conclusion

It can be concluded that the line structure distinguishable in the constructed spectra of atmospheric pressure and temperature variations with periods ranging from 10 days to 10 years reflect real physical processes that remain periodic (coherent) for tens of years.

Spectral lines should be thoroughly distinguished and quantified to be suitable for predicting the majority of variations with a time resolution of 10 days and reliably forecasting climate changes for tens of years in advance. The existing practice of smoothing these lines and adjusting the available observational data to a representation in terms of a random process leads to the loss of useful information.

Prognosis of pressure variations provides a solid basis on which to forecast weather and climate changes caused, in the first place, by astronomical factors. The elucidation of the nature of spectral lines can make it possible to use astronomical observations of planetary motions to improve the accuracy of forecasting. The intense planetary action on the Earth, which does not reduce to gravitational effects, influences atmospheric processes and thus induces climatic variations. The mechanism of this action consists of the modulation of the solar-energy flux due to oscillations in the orbital position of the Earth. This action is seriously perverted by the Earth's rotation, which leads to additional climatic variations not only at the harmonics of the planet's synodic period but also at the first combination of these harmonics with the frequency of the Earth's revolution around the Sun.

An interesting physical fact described in this review is the marked difference between the periods of the Earth's orbital revolution and oscillations in the distance between the Earth and the Sun. These processes are involved in the formation of line *S*. This should be a composite line containing two complex peaks and resembling line *Mm* related to the Moon's motion. In the context of a study of this phenomenon, it is of great interest to analyze sea-level-fluctuation spectra using periods of 100 and 200 years, which could make it possible to resolve the components of the peak and accurately determine the period of radial oscillations, the astronomical estimate of which appears doubtful.

Some of the above findings can be used in the research practice.

1. The understanding of the periodic nature of climatic variations with the most intense fluctuations at the periods of Jupiter's revolution (11.8 years) and regression of lunar orbital nodes (18.6 years) may be useful in analyzing the age of Holocene deposits to develop methods for tracing geologic catastrophes. It is this finding that seems to be the most valuable result of this study. These periodic variations were considered in the corresponding section of this review.

2. Fine-structure analysis of the spectral lines of tidal variations at the lunar rotation frequency contributes to a more accurate evaluation of lunar motion and can be used in astronomy for studies of the Moon's orbital evolution [38].

3. Also important for future research is the possibility of comparing spectral-line amplitudes of atmospheric-pressure and sea-level variations. The amplitude ratios may differ considerably, but most of them concentrate near two values, 1 $mbar^2\ cm^2$ and 0.3 $mbar^2\ cm^{-2}$. The classification of lines based on this characteristic allows the origin of fluctuations to be identified as atmospheric or oceanic [39].

Acknowledgements. The author thanks J Y Chung (Seoul National University) for tis support of this work.

Thanks are also due to Aota (Sapporo, Japan), S I Varlamov (Fukuoka, Japan), V M Pishchal'nik (Pacific Research Institute of Fisheries and Oceanography, Sakhalin, Russia), Yu Kato (Russian Committee for Hydrometeorology and Environmental Control, Sakhalin, Russia), and M I Strel'tsov (Institute of Marine Geology and Geophysics, Yuzhno-Sakhalinsk, Russia) for providing materials of observation.

References

1. Bowden K F *Physical Oceanography of Coastal Waters* (Chichester: E. Horwood, 1983) [Translated into Russian (Moscow: Mir, 1988)]
2. Nalimov V V, Drogalina Zh A *Real'nost' Nereal'nogo: Veroyatnostnaya Model' Bessoznatel'nogo* (Reality of the Unreal: Probabilistic Model of the Unconscious) (Moscow: Mir Ideĭ, AO "AKRON", 1995)
3. Monin A S *Gidrodinamika Atmosfery, Okeana i Zemnykh Nedr* (Hydrodynamics of the Atmosphere, Ocean, and Interior of the Earth) (St. Petersburg: Gidrometeoizdat, 1999)
4. Chung J Y, Ivanova K V, Ivanov V V, in *Abstracts of the 1996 Spring Meeting at PUSAN* (Pusan: The Korean Society of Oceanography, 1996) p. 29
5. Evanova E V, Ivanov V V, Chung J Y, in *Proc. of the 10st RIO – RIAM Joint Workshop on "Sea Level Variations in the Adjacent Seas of Korea"* (Seoul: Research Institute of Oceanography, Seoul National University, 1999) p. 3
6. Poezzhalova O S, Shevchenko G V, in *Geodinamika Tektonosfery Zony Sochleneniya Tikhogo Okeana s Evrazieĭ* Vol. VII (Geodynamics of the Tectonosphere at the Junction of the Pacific Ocean and Eurasia) (Ed V M Kaĭstrenko) (Yuzhno-Sakhalinsk: Isd. DVO RAN, 1999) p. 131
7. Lamb H *Hydrodynamics* (Cambridge: The Univ. Press, 1932)
8. Swarztrauber P, Sweet R "Efficient FORTRAN subprograms for the solution of elliptic partial differential equations", NCAR Tech. Note NCAR-TN/IA-109 (Boulder, CO: National Center for Atmospheric Research, 1975)
9. Kahaner D K *Z. Angew. Math. Phys.* **29** 397 (1978)
10. Kahaner D, Moler C, Nash S *Numerical Methods and Software* (Englewood Cliffs, NJ: Prentice Hall, 1989) [Translated into Russian (Moscow: Mir, 2001) p. 481]
11. D'yakonov V P *Maple 6*. Uchebnyĭ Kurs (Maple 6. Training Course) (St. Petersburg: Piter, 2001)
12. D'yakonov V P *MATHLAB 6*. Uchebnyĭ Kurs (MATHLAB 6. Training Course) (St. Petersburg: Piter, 2001)
13. D'yakonov V P *Mathematica 4*. Uchebnyĭ Kurs (Mathematica 4. Training Course) (St. Petersburg: Piter, 2000)
14. Woodward Ph M *Probability and Information Theory, with Applications to Radar* (London: Pergamon Press, 1953) [Translated into Russian (Moscow: Sov. radio, 1961)]
15. Cooper G R, McGillem C D *Probabilistic Methods of Signal and System Analysis* (New York: Holt, Rinehart, and Winston, 1971) [Translated into Russian (Moscow: Mir, 1989)]
16. Marchuk G I, Kagan B A *Dinamika Okeanskikh Prilivov* (Dynamics of Oceanic Tides) (Leningrad: Gidrometeoizdat, 1983) [Translated into English: *Dynamics of Ocean Tides* (Dordrecht: Kluwer Acad. Publ., 1989)]
17. Patullo J G et al. *J. Mar. Res.* **14** 88 (1955)
18. LeBlond P H, Mysak L A *Waves in the Ocean* (Amsterdam: Elsevier Sci. Publ. Co., 1978) [Translated into Russian (Moscow: Mir, 1981)]
19. Humphreys W J *Physics of the Air* 2nd ed. (New York: McGraw-Hill Book Co., 1929) [Translated into Russian (Moscow: ONTI, 1936)]
20. Struve O, Lynds B, Pillans H *Elementary Astronomy* (New York: Oxford Univ. Press, 1959) [Translated into Russian (Moscow: Nauka, 1964)]
21. *Astronomicheskiĭ Ezhegodnik SSSR na 1983 God* (USSR Astronomical Year-Book for the year 1983) (Leningrad: Nauka, 1980)
22. Kaye G W C, Laby T H *Tables of Physical and Chemical Constants and Some Mathematical Functions* 12th ed. (London: Longmans, 1959) [Translated into Russian (Moscow: Fizmatgiz, 1962)]
23. Arnol'd V I *Dopolnitel'nye Glavy Teorii Obyknovennykh Differentsial'nykh Uravneniĭ* (Additional Chapters to the Theory of Ordinary Differential Equations) (Moscow: Nauka, 1978) [Translated into English: *Geometrical Methods in the Theory of Ordinary Differential Equations* (New York: Springer-Verlag, 1983)]
24. Roy A E *Orbital Motion* (Bristol: Hilger, 1978) [Translated into Russian (Moscow: Mir, 1981)]

25. Landau L D, Lifshitz E M *Mekhanika* (Mechanics) (Moscow: Nauka, 1973) [Translated into English (Oxford: Pergamon Press, 1976)]
26. Milankovitch M *Mathematische Klimalehre und astronomische Theorie der Klimaschwankungen* (Berlin, 1930) [Translated into Russian (Moscow – Leningrad: GONTI, 1939)]
27. Monin A S *Vrashchenie Zemli i Klimat* (Earth's Rotation and Climate) (Leningrad: Gidrometeoizdat, 1972) [Translated into English (Delhi: Radok-Radhakrishna, 1974)]
28. Darwin G H *The Tides and Kindred Phenomena in the Solar System* (San Francisco: W.H. Freeman, 1962) [Translated into Russian (Moscow: Nauka, 1965)]
29. Dobrand W et al. *Praxis der Fortran-Programmierung reiche Automatisierentechnik* (Berlin: VEB Verlag, 1971) [Translated into Russian (Moscow: Statistika, 1973)]
30. Shul'gin M F, Litenko N L, Genesina A S *Klimat Yuzhno-Sakhalinska* (Climate of the City of Yuzno-Sakhalinsk) (Leningrad: Gidrometeoizdat, 1982)
31. Klimov S M, in *Nestatsionarnye Dlinnovolnovye Protsessy na Shel'fe Kuril'skikh Ostrovov* (Nonstationary Long-Wave Processes on the Shelf of the Kuril Islands) (Eds V M Kaĭstrenko, A B Rabinovich) (Vladivostok: Izd. DVNTs AN SSSR, 1984) p. 128
32. Aota M, PICES Scientific Report No. 12 (Sidney, BC, Canada: PICES, 1999) p. 1
33. Richter-Bernburg G, in *Problems in Palaeoclimatology: Proc. of the NATO Palaeoclimates Conf., 1963* (Ed. A E M Nairn) (London: Interscience Publ., 1964) p. 510 [Translated into Russian: *Problemy Paleoklimatologii* (Nauki o Zemle. Fundamental'nye Trudy Zarubezhnykh Uchenykh po Geologii, Geofizike i Geokhimii, T. 6) (Moscow: Mir, 1968) p. 336]
34. Shostakovich B V, in *Zapiski Gosudarstvennogo Gidrologicheskogo Instituta* (Transactions of the State Hydrological Institute) (Leningrad: GGI, 1934) p. 13
35. Currie R G *J. Coastal Res.* (Special issue 17) 29 (1991)
36. Ivanov V V, in *Otchet Instituta Morskoĭ Geologii i Geofiziki DVO RAN. 1998. Kuril'skaya Programma* (Report of the Institute of Marine Geology and Geophysics, Far-Eastern Branch of the Russian Academy of Sciences, 1998. Kuril Program) (Yuzhno-Sakhalinsk: Izd. IMGiG DVO RAN, 1998) p. 26
37. Igarashi Y et al., in *Proc. of the 16th Intern. Symp. on Okhotsk Sea and Sea Ice, 4–8 Feb. 2001, Mombetsu, Hokkaido, Japan* (Mombetsu: Cold Ocean Research Association, 2001) p. 228; Yanagi T, in *Proc. of the 10st RIO-RIAM Joint Workshop ob* "*Sea Level Variations in the Adjacent Seas of Korea*" (Seoul: Research Institute of Oceanography, Seoul National University, 1999) p. 1
38. Morrison L V *Moon* **5** 253 (1972) [Translated into Russian: in *Prilivy i Rezonansy v Solnechnoĭ Sisteme* (Tides and Resonances in the Solar System) (Ed. V N Zharkov) (Moscow: Mir, 1975) p. 273]
39. Lappo S S, Skripnik A V, Likhacheva O N *Dokl. Akad. Nauk SSSR* **244** 1475 (1979)